EUROPEAN ORGANIZATION FOR NUCLEAR RESEARCH (CERN)

CERN-PH-EP/2015-170
2016/06/20

CMS-B2G-13-006

Search for pair-produced vectorlike B quarks in proton-proton collisions at $\sqrt{s} = 8\,\text{TeV}$

The CMS Collaboration*

Abstract

A search for the production of a heavy B quark, having electric charge $-1/3$ and vector couplings to W, Z, and H bosons, is carried out using proton-proton collision data recorded at the CERN LHC by the CMS experiment, corresponding to an integrated luminosity of $19.7\,\text{fb}^{-1}$. The B quark is assumed to be pair produced and to decay in one of three ways: to tW, bZ, or bH. The search is carried out in final states with one, two, and more than two charged leptons, as well as in fully hadronic final states. Each of the channels in the exclusive final-state topologies is designed to be sensitive to specific combinations of the B quark-antiquark pair decays. The observed event yields are found to be consistent with the standard model expectations in all the final states studied. A statistical combination of these results is performed, and upper limits are set on the cross section of the strongly produced B quark-antiquark pairs as a function of the B quark mass. Lower limits on the B quark mass between 740 and 900 GeV are set at a 95% confidence level, depending on the values of the branching fractions of the B quark to tW, bZ, and bH. Overall, these limits are the most stringent to date.

Published in Physical Review D as doi:10.1103/PhysRevD.93.112009.

*See Appendix A for the list of collaboration members

1 Introduction

The discovery of a Higgs boson [1–3] has intensified the search for physics beyond the standard model (SM). Various extensions of the SM predict the existence of new heavy quarks, which arise quite naturally in grand unification schemes [4] and in composite Higgs [5, 6], little Higgs [7–10], and top quark condensate [11] models. The couplings to the SM gauge bosons of the left- and right-handed components of these quarks are symmetric, so they are called vectorlike [12]. Vectorlike quarks may be singlets, doublets, or triplets under the electroweak $SU(2) \times U(1)$ transformation [13]. They have bare mass terms that are invariant under the electroweak gauge transformation [14]. Moreover, their couplings to the scalar sector are independent of mass. Thus, the existence of vectorlike quarks is not ruled out by the recent discovery of a Higgs boson, in contrast to additional quarks in more conventional fourth-generation models [15].

In several beyond the standard model scenarios, vectorlike quarks are considered partners of the top and bottom quarks [16]. Both the charged-current [17] and the flavor changing neutral current (FCNC) [18, 19] decay processes are allowed. The ratio of the predicted rates depends on the model: in some models the FCNC process dominates [20]; in others the two modes are comparable in rate.

This paper describes the search for a vectorlike B quark of electric charge $-1/3$, using data recorded by the CMS experiment from proton-proton collisions at a center-of-mass energy of 8 TeV at the CERN LHC in 2012. It is assumed that B quark-antiquark pairs are produced strongly for B quark masses within the range of this search, which extends to 1 TeV. The B quark may decay either via the charged-current process $\mathrm{B} \to \mathrm{tW}$ or via the FCNC processes $\mathrm{B} \to \mathrm{bZ}$ and $\mathrm{B} \to \mathrm{bH}$. Feynman diagrams for the B quark pair production and decay processes are shown in Fig. 1. Searches are performed in several different final states, including those containing single leptons, lepton pairs (dileptons) of opposite or identical charge, three or more leptons, or consisting entirely of hadronic activity without any identified leptons. We search for an excess of events over the backgrounds in mutually exclusive final states and set limits on the pair-production cross section for all values of the B quark branching fractions with the constraint $\mathcal{B}(\mathrm{B} \to \mathrm{tW}) + \mathcal{B}(\mathrm{B} \to \mathrm{bZ}) + \mathcal{B}(\mathrm{B} \to \mathrm{bH}) = 1$.

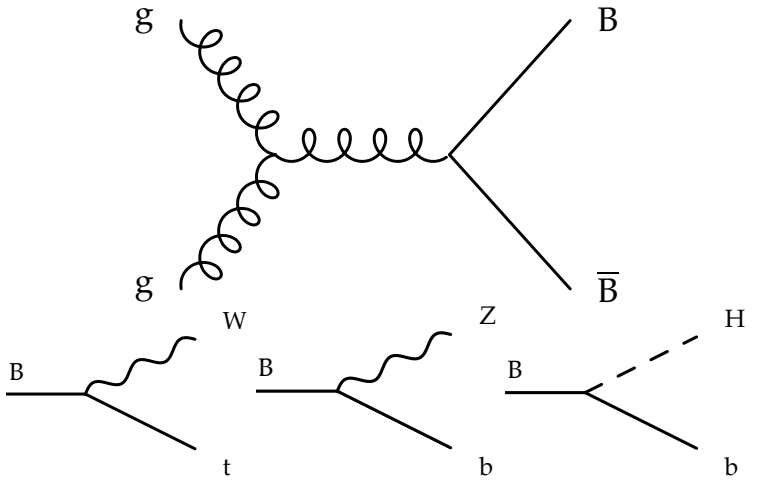

Figure 1: Feynman diagrams for the dominant B quark pair-production process (top) and for the B quark decay modes (bottom).

Experimental searches for a vectorlike B quark have previously been reported by experiments at the Fermilab Tevatron and the CERN LHC. A 95% CL lower limit on the mass of the B

quark was set at 268 GeV by the CDF Collaboration [21]. Recently the ATLAS Collaboration set lower limits on the B quark mass ranging from 575 to 813 GeV, for different combinations of the B quark branching fractions [22]. The present analysis improves upon these existing results, setting the most stringent limits to date on the mass of the vectorlike B quark.

The paper is divided into several sections. Section 2 gives an overview of the CMS detector. Section 3 describes the details of the simulations used for signal and background processes. Section 4 describes the reconstruction of physics objects and the event selections specific to each individual channel considered in this analysis. Section 5 describes background estimation techniques for each of the channels, as well as the specific methods used to discriminate the B quark signal from the background, while Sec. 6 describes the systematic uncertainties evaluated for each channel and their treatment in combination. Finally, Sec. 7 provides further details on the combination of analysis channels and Sec. 8 presents the results obtained from this analysis. A summary is presented in Sec. 9.

2 CMS detector

The central feature of the CMS apparatus is a superconducting solenoid of 6 m internal diameter, providing a magnetic field of 3.8 T. Within the solenoid volume are a silicon pixel and strip tracker, a lead tungstate crystal electromagnetic calorimeter (ECAL), and a brass and scintillator hadron calorimeter, each composed of a barrel and two end cap sections. Muons are measured in gas-ionization detectors embedded in the steel flux-return yoke outside the solenoid. Extensive forward calorimetry complements the coverage provided by the barrel and end cap detectors. The first level of the CMS trigger system, composed of custom hardware processors, uses information from the calorimeters and muon detectors to select the most interesting events in a fixed time interval of less than 4 μs. The high-level trigger processor farm further decreases the event rate from around 100 kHz (the maximum allowed output from the first level) to around 400 Hz, before data storage. A more detailed description of the CMS detector, together with a definition of the coordinate system used and the relevant kinematic variables, can be found in Ref. [23].

3 Signal and background simulation

The following section details the simulation methods used to generate events for modeling the signal and background processes. One of the main backgrounds in many of the channels is SM $\mathrm{t\bar{t}}$ production. This process is simulated with the MADGRAPH v5.1.1 event generator [24], using the CTEQ6L1 parton distribution function (PDF) [25]. Events are interfaced with PYTHIA v6 [26] for shower modeling and hadronization. These simulation methods are used for the W+jets and Z+jets samples, in addition to SM $\mathrm{t\bar{t}}$ production. For W+jets and Z+jets events, up to four additional partons are allowed at the matrix element level during generation.

Diboson processes WW, WZ, and ZZ are generated with PYTHIA 6.424, and single top quark processes (tW, s-channel, and t-channel) are generated using POWHEG 1.0 [27–30] and interfaced with PYTHIA for shower modeling and hadronization. Both the diboson and single top processes are generated with the CTEQ6M PDF set. The rare processes $\mathrm{t\bar{t}W}$, $\mathrm{t\bar{t}Z}$, and $\mathrm{t\bar{b}Z}$ are simulated with MADGRAPH v5.

Normalizations for the background processes are initially set according to theoretical predictions, and are allowed to vary within the corresponding uncertainties during cross section limit extraction. For W+jets and Z+jets processes, we use the calculations found in Refs. [31–33]. For

$t\bar{t}$ and single top samples, we normalize using cross sections calculated in Refs. [34] and [35], respectively. Finally, for diboson and rare processes we use cross sections computed in Refs. [36] and [37, 38], respectively.

To model the kinematic properties of the $pp \to B\overline{B}$ signal process, we use samples of simulated events produced with the MADGRAPH v5 generator and CTEQ6L1 PDF set, allowing for up to two additional partons in the final state of the hard scatter matrix element. The generated events are then interfaced with PYTHIA v6 for parton shower modeling and hadronization.

Samples are generated for B quark masses between 500 and 1000 GeV, in steps of 50 GeV, for each of the six distinct combinations of decay products: tWtW, tWbZ, tWbH, bZbZ, bHbZ, and bHbH. The standard model final states identical to those listed here are not considered, as the rates are negligible relative to the other background processes. By reweighting events from these different samples, an arbitrary combination of branching fractions to tW, bZ, and bH can be probed. To normalize the simulated samples to expected event yields, we use cross sections computed to next-to-next-to-leading order (NNLO) using both HATHOR [39] and TOP++2.0 [40]. The numerical values used for the B quark pair-production cross sections as a function of mass, generated with TOP++2.0, are listed in Table 1.

Table 1: Production cross sections for $pp \to B\overline{B}$, used to normalize simulated signal samples to expected event yields. The cross sections are computed to NNLO with Top++2.0 [40].

M(B) [GeV]	Cross section σ [pb]
450	1.153
500	0.590
550	0.315
600	0.174
650	0.0999
700	0.0585
750	0.0350
800	0.0213
850	0.0132
900	0.00828
950	0.00525
1000	0.00336

Finally, to reproduce the LHC running conditions, simulated events are reweighted to match the observed distribution of the number of reconstructed primary vertices per bunch crossing in data.

4 Event reconstruction

Events from the LHC collision data or from simulation are reconstructed using the particle flow (PF) algorithm [41, 42], which collects information from all subdetectors to reconstruct all detected particles in an event. Events are required to have at least one reconstructed vertex. The interaction vertex with the largest sum of the transverse momentum squared p_T^2 of associated tracks is considered the primary interaction vertex. Charged particles originating from other vertices due to additional inelastic proton-proton collisions within the same bunch crossing (pileup) are rejected.

Electron candidates are reconstructed from clusters of energy deposited in the ECAL matched to charged particle trajectories identified in the tracker [43]. Electrons and muons with p_T above

30 GeV and pseudorapidity $|\eta| < 2.4$ are accepted, excluding electrons with $1.44 < |\eta| < 1.57$, in the transition region between the ECAL barrel and end cap. The muon candidates are reconstructed using information from the tracker and the muon spectrometer. Muon candidates are required to have only a small amount of energy deposited in the calorimeters. Further quality requirements are imposed on the muon tracks and the fit to the matched segments in the muon detectors [44]. Only tracks originating from the primary interaction vertex are considered.

Electron and muon candidates are reconstructed and identified based on quality selection requirements, while hadronically decaying tau leptons (τ_h) are identified using the Hadron Plus Strip (HPS) [45] algorithm, which relies on hadrons and photons to construct the various tau lepton hadronic decay modes. The HPS PF tau leptons are required to have $p_T > 20$ GeV and $|\eta| < 2.3$. Additionally, we require τ_h to be separated by $\Delta R = \sqrt{(\Delta\eta)^2 + (\Delta\phi)^2} > 0.1$ from electron and muon candidates, where ϕ is the azimuthal angle.

The isolation of the lepton candidates (including electrons, muons, and decays of tau leptons to electrons or muons) is measured by the activity in a cone of aperture ΔR around the lepton direction at the primary vertex. The p_T of charged particles originating at the primary vertex and the p_T of the neutral particles and photons are summed in this cone (excluding the lepton candidate itself) to obtain the isolation variable. Contributions to the neutral hadron and photon energy components due to pileup interactions are subtracted. For the electron isolation, this contribution is determined using the jet area technique [46], which computes the transverse energy density of neutral particles using the median of the neutral energy distribution in a sample of jets with $p_T > 3$ GeV. In the case of the muons, the pileup energy density from neutral particles is estimated to be half of that from charged hadrons, based on measurements performed in jets [47]. The difference between the isolation algorithms arises because electrons and muons are reconstructed using different techniques. Electrons, with large energy deposition in the calorimeters, behave similarly to jets in this respect, while the reconstruction of muons relies more heavily on tracking information. The isolation value, defined as the energy reconstructed in a cone of $\Delta R = 0.3$ (0.4) around an electron (muon) candidate, is required to be less than 0.15 (0.12) times the electron (muon) p_T for the lepton to be considered isolated. The lepton identification and isolation conditions remove most of the nonprompt lepton backgrounds.

Particles are clustered to form hadronic jets using the anti-k_T algorithm [48] with a distance parameter of 0.5. Throughout this paper such clusters are referred to as AK5 jets. The AK5 jets with $p_T > 30$ GeV and $|\eta| < 2.4$ are selected, with further requirements that the jet has at least two associated tracks and that at least 1% of the jet energy fraction is measured in the calorimeters, to remove poorly reconstructed jets. Jet energy corrections are applied; these are derived from simulation and are matched to measurements in data [49].

Jets arising from the hadronization of b quarks (b jets) are identified using the combined secondary vertex (CSV) b-tagging algorithm [50], which uses information from tracks and secondary vertices associated with jets to compute a likelihood-based discriminator to distinguish between jets from b quarks and those from charm or light quarks and gluons. The b-tagging discriminator returns a value between 0 and 1, with higher values indicating a higher probability of the jet to originate from a bottom quark. A discriminator threshold is chosen which gives a b-tagging efficiency of about 70%, with a mistagging rate of about 1.5% for jets originating from light-flavor quarks or gluons with p_T in the range of 80–120 GeV. The b-tagging efficiency is measured in data and simulation, and corrections are applied to simulated events to account for any differences, as a function of p_T and η [51]. The missing transverse momentum vector is defined as the projection on the plane perpendicular to the beams of the negative vector sum of the momenta of all reconstructed particles in an event. Its magnitude is referred to as $\not{E}_T$. The

quantity S_T is defined as the scalar sum of the p_T of the jets, lepton p_T, and $\not{E}_T$ in the event.

At very high Lorentz boost, the products of hadronically decaying bosons may be merged into a single reconstructed jet. In this regime, the W, Z, or Higgs bosons are identified as jets clustered with the Cambridge-Aachen algorithm [52, 53] using a larger distance parameter of 0.8 [54]. In this paper, they are referred to as CA8 jets. For bosons with p_T above approximately 200 GeV, decay products are expected to be clustered into a single CA8 jet. Each CA8 jet can be decomposed into constituent subjets using a jet pruning algorithm [55] to resolve those decay products. The pruning algorithm removes soft and wide-angle components of the jet during a reclustering, and the last iteration of the clustering process is reversed to identify two subjet candidates within each pruned jet. Jet properties such as jet mass, N-subjettiness [56] (used to determine the consistency of a jet with N hypothesized subjets), and the mass drop, defined as the ratio of the most massive subjet to the mass of the pruned jet, are used to identify these bosons.

The trigger selection for each channel entering the combination can be different, depending on the final state of interest. For the single-lepton channel, two trigger selections are utilized: either a single electron with $p_T > 27$ GeV or a single muon with $p_T > 40$ GeV. For both of the lepton pair channels, as well as the multilepton channel, three trigger algorithms are used for final states including two electrons, two muons, or one electron and one muon. In each of these dilepton trigger algorithms, events are selected if the highest-p_T lepton has $p_T > 17$ GeV and the second-highest p_T lepton has $p_T > 8$ GeV. No charge requirement is applied in the trigger selection, allowing these trigger algorithms to be used in all three channels with two or more leptons. Finally, the all-hadronic channel uses a trigger algorithm requiring the total scalar p_T sum of reconstructed jets (with $p_T > 30$ GeV and $|\eta| < 3.0$) in the detector to be greater than 750 GeV. The offline requirements for each channel of the analysis are designed to be fully efficient given these trigger requirements. Differences in the trigger selections used between analysis channels lead to small differences in the total amount of integrated luminosity utilized in each channel.

The details of the event selections for each individual analysis channel are given in the following subsections. Table 2 summarizes these channels in terms of their defining characteristics: the number of selected leptons, the discriminating variable used for limit setting, as well as the decay mode of the B quark for which the channel is most sensitive.

Table 2: A summary of analysis channels entering the combination, along with the number of selected leptons, the variable used for signal discrimination, and the B quark decay mode providing the best sensitivity for the channel.

	Number of leptons	Discriminating variable	Best decay mode
Lepton+jets	1	S_T	tW
Same-sign dilepton	2	S_T	tW
Opposite-sign dilepton	2	$M(\ell\ell\,\mathrm{b})$	bZ
Multilepton	$\geq$3	S_T	tW, bZ
All-hadronic	0	H_T	bH

4.1 Lepton+jets channel

Charged leptons from the decays of W and Z bosons are selected using the criteria described in Sec. 4, and are required to be isolated from jets. The lepton trajectories are also required to have a transverse impact parameter of less than 0.02 cm and a longitudinal impact parameter of less than 1 cm in magnitude, relative to the primary vertex. The final selection requires events to

have exactly one isolated lepton and at least four jets with $p_T > 200, 60, 40, 30$ GeV, respectively, of which at least one is a bottom jet. The minimum number of jets and the jet p_T requirements are selected to enhance sensitivity to the $B\overline{B}$ signal with $B \to tW$ decays. To further suppress the SM backgrounds, we use the centrality, C, defined as the scalar sum of the p_T of the jets divided by the scalar sum of the jet energies, requiring $C > 0.4$. We require events to have $\not{E}_T > 20$ GeV. Corrections due to differing trigger, lepton, and b jet identification efficiencies in data and simulation are applied to simulated events.

Events are divided into categories containing 0, 1, or $\geq$2 tagged hadronically decaying W, Z, or Higgs bosons using the CA8 jets. The identification criteria for these signatures require the CA8 jet to have p_T greater than 200 GeV and to be matched to an AK5 jet. The AK5 jets matched to CA8 jets are then excluded from b-tagging requirements. The two subjets identified with the pruning algorithm [55] are required to have an invariant mass between 50 and 150 GeV, to be consistent with a W, Z, or Higgs boson. To further reduce SM backgrounds, the mass drop is required to be less than 0.4. The efficiency of this heavy-boson tagging algorithm is approximately 50% [57], and correction factors are applied to compensate for efficiency differences between data and simulation. To discriminate the B quark signal from the expected backgrounds, the S_T distribution is used.

4.2 Same-sign lepton pair channel

Events enter the same-sign (SS) dilepton channel if they contain two leptons (ee, $\mu\mu$, and eμ) having the same electric charge. Events containing an additional reconstructed electron, muon, or tau lepton candidate are removed from the final selection. This channel is optimized for $B \to tW$ decays, but maintains some sensitivity for bZ and bH decays. In events with a top quark and a W boson, high hadronic activity is expected in addition to the lepton pair, and therefore events are included in the signal region only if they contain four or more jets in addition to the lepton pair.

In this channel the B quarks are not fully reconstructed. Instead, to discriminate signal from background, the S_T distribution is used. Events with $\not{E}_T > 30$ GeV are categorized into five S_T bins (0.2–0.4, 0.4–0.6, 0.6–0.8, 0.8–1.2, and $S_T > 1.2$ TeV) for each of the dilepton channels.

4.3 Opposite-sign lepton pair channel

In this channel, optimized for the B decaying to a Z boson and b quark, the Z boson candidates are reconstructed from pairs of electrons or muons having opposite electric charge, with the identification and isolation criteria previously described. The two highest p_T leptons of the same flavor but opposite charge are used. The pairwise invariant mass of these two objects, $M(\ell\ell)$, where ℓ represents an electron or a muon, is required to be in the range of 60–120 GeV, consistent with lepton pairs originating from a Z boson decay. Furthermore, the $Z \to \ell^+\ell^-$ candidates are required to have $p_T(\ell\ell) > 150$ GeV. Events are further required to have at least one b jet with $p_T > 80$ GeV. The requirements are optimized to select Z bosons and b jets originating from the decay of a heavy B quark (>500 GeV), where the decay products are expected to have large p_T. The kinematic properties of one B quark are reconstructed from the Z boson and the highest-p_T b jet, with $M(\ell\ell b)$ used to discriminate the B quark signal. The invariant mass distributions of the B quark candidates for different $M(B)$ are shown in Fig. 2. A signal peak can be identified over a continuous falling background. This reconstruction strategy allows the other B quark from the $B\overline{B}$ quark-antiquark pair to decay into bZ, bH, or tW.

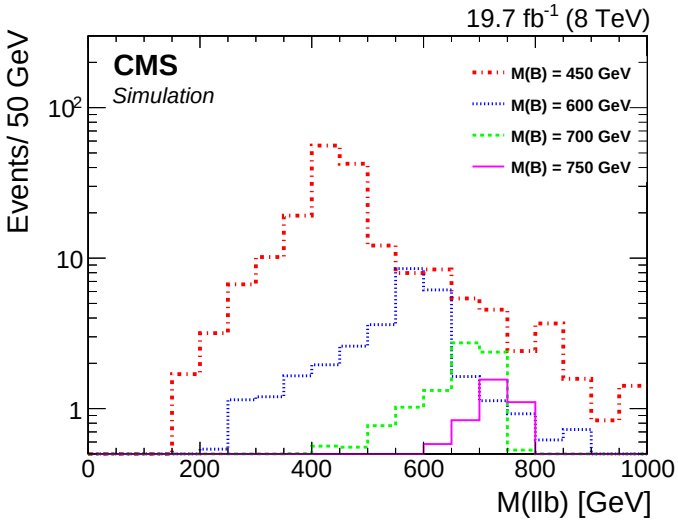

Figure 2: The reconstructed mass of the B quark candidate in the opposite-sign lepton pair channel, using the invariant mass of the dilepton and b jet in simulated events.

4.4 Multilepton channel

Events in this channel must have at least three leptons, consisting of electrons, muons, or tau leptons decaying into fully hadronic states (τ_h). The highest p_T (leading) electron or muon is required to have $p_T > 20\,\text{GeV}$ and the subleading leptons are required to have $p_T > 10\,\text{GeV}$. The p_T selection criteria are chosen such that the triggers are fully efficient on these events.

We sort multilepton events into exclusive categories based on the number of leptons, lepton flavor, and relative charges, as well as the kinematic quantity S_T. First, we separate events containing hadronically decaying tau leptons, as their reconstruction is less efficient and this results in lower-purity categories.

Next, we classify each event in terms of the maximum number of opposite-sign and same-flavor (OSSF) lepton pairs that can be made by using each lepton only once. For example, both $\mu^+\mu^-\mu^-$ and $\mu^+\mu^-e^-$ contain only one pair of OSSF leptons and are denoted OSSF1, $\mu^+\mu^+e^-$ contains no such OSSF pair and is denoted OSSF0, while $\mu^+\mu^-e^+e^-$ contains two such pairs and is denoted OSSF2. Thus orthogonal categories of events are defined that contain 0, 1, or 2 OSSF lepton pairs. These categories are further divided, depending on whether or not a lepton pair has $M(\ell\ell)$ in the range 75–105 GeV, consistent with a Z boson decay. Same-flavor dilepton pairs consistent with low-mass resonances are excluded from the search region with a requirement of $M(\ell\ell) > 12\,\text{GeV}$.

4.5 All-hadronic channel

The final channel contributing to the search for B quarks includes events reconstructed in an all-hadronic topology, to increase sensitivity to the bH decay mode of the B vectorlike quark. The search in this channel is designed for Higgs bosons decaying to a pair of b quarks. Because of the high mass of the B quark, the Higgs boson is expected to be highly Lorentz boosted; consequently the b quarks from the Higgs boson decay have a small angular separation. To reconstruct this signature, jet substructure algorithms are used. The Higgs boson is reconstructed using a single CA8 jet. This jet is required to have $p_T > 300\,\text{GeV}$. The pruned jet mass is required to be in the range $90 < M(\text{jet}) < 140\,\text{GeV}$, to be consistent with the Higgs boson mass. The N-subjettiness observables τ_2 and τ_1 [56] are used to further increase the purity of events containing the two-prong decay of the Higgs boson in the $H \to b\bar{b}$ decay mode. We require

the condition $\tau_2/\tau_1 < 0.5$ to ensure that jets containing two distinct deposits of energy (subjets) are selected as the $H \to b\bar{b}$ candidates. Finally, the two identified subjets are required to be individually b tagged using the CSV algorithm. Jets satisfying all of these criteria are known as H-tagged jets. At least one reconstructed H-tagged jet is required for the final event selection.

Events are also required to have at least one additional b-tagged jet, to reconstruct the b quark originating directly from the B quark decay. Events are categorized according to the number of b-tagged jets: exactly one or at least two. To further reduce background contributions to the event selection, a requirement is made on H_T, defined for this channel as the scalar p_T sum of all AK5 jets with p_T above 50 GeV. A requirement of $H_T > 950$ GeV maintains a high signal sensitivity while eliminating most of the multijet background.

5 Estimation of backgrounds

In this section we describe the variety of the methods used to estimate the background contributions for each of the channels contributing to the search. Detailed descriptions of the systematic uncertainties applied to these methods, and shown in the figures presented here, can be found in Sec. 6.

5.1 Lepton+jets channel

The dominant background contribution to the lepton+jets analysis is SM top quark pair production, accounting for 77% of the expected background yield. Other processes also contribute, including W/Z+jets, single top quark, diboson, and $t\bar{t}$ plus vector boson production, which together account for 17% of the expected background yield. The electroweak backgrounds are taken from simulation. The remaining contribution to the background estimation is due to multijet events. To model and estimate the contribution from these processes, control samples in data are used. The S_T shape is taken from a multijet-enriched region defined by the selection of nonisolated leptons, or in the case of electrons, those failing the identification criteria. The S_T shapes from nonisolated leptons and isolated leptons were compared for several kinematic selections in both channels and were found to be consistent. The normalization is obtained by fitting the $\not{E}_T$ distribution in data individually in the 0, 1, and $\geq$ 2 boson categories. The electroweak backgrounds are constrained to their expected cross sections and allowed to float within uncertainties, while the multijet normalization is allowed to float freely in these fits.

Events are categorized based on the flavor of the identified lepton, as well as the number of identified heavy-boson-tagged jets (V tags), including 0, 1, and $\geq$2. Figure 3 shows the S_T distributions for these categories, which are used for signal discrimination in this channel.

5.2 Same-sign lepton pair channel

The background contributions for the dilepton channel with same-sign leptons are divided into distinct categories. The first category includes events with two prompt leptons having the same charge. This category of events represents an irreducible background composed of various SM processes, including $t\bar{t}W$, $t\bar{t}Z$, diboson, and triboson production. These background contributions are modeled using simulated events.

A second category of background events arises when the charge of one of the leptons from an oppositely charged pair is mismeasured, which happens most frequently in the same-sign ee channel. To model this contribution, the charge misidentification rate is measured using a control sample enhanced in Z+jets and $t\bar{t}$ events having two leptons in the final state. The charge misidentification rate is extracted from the ratio of the number of events in this selection

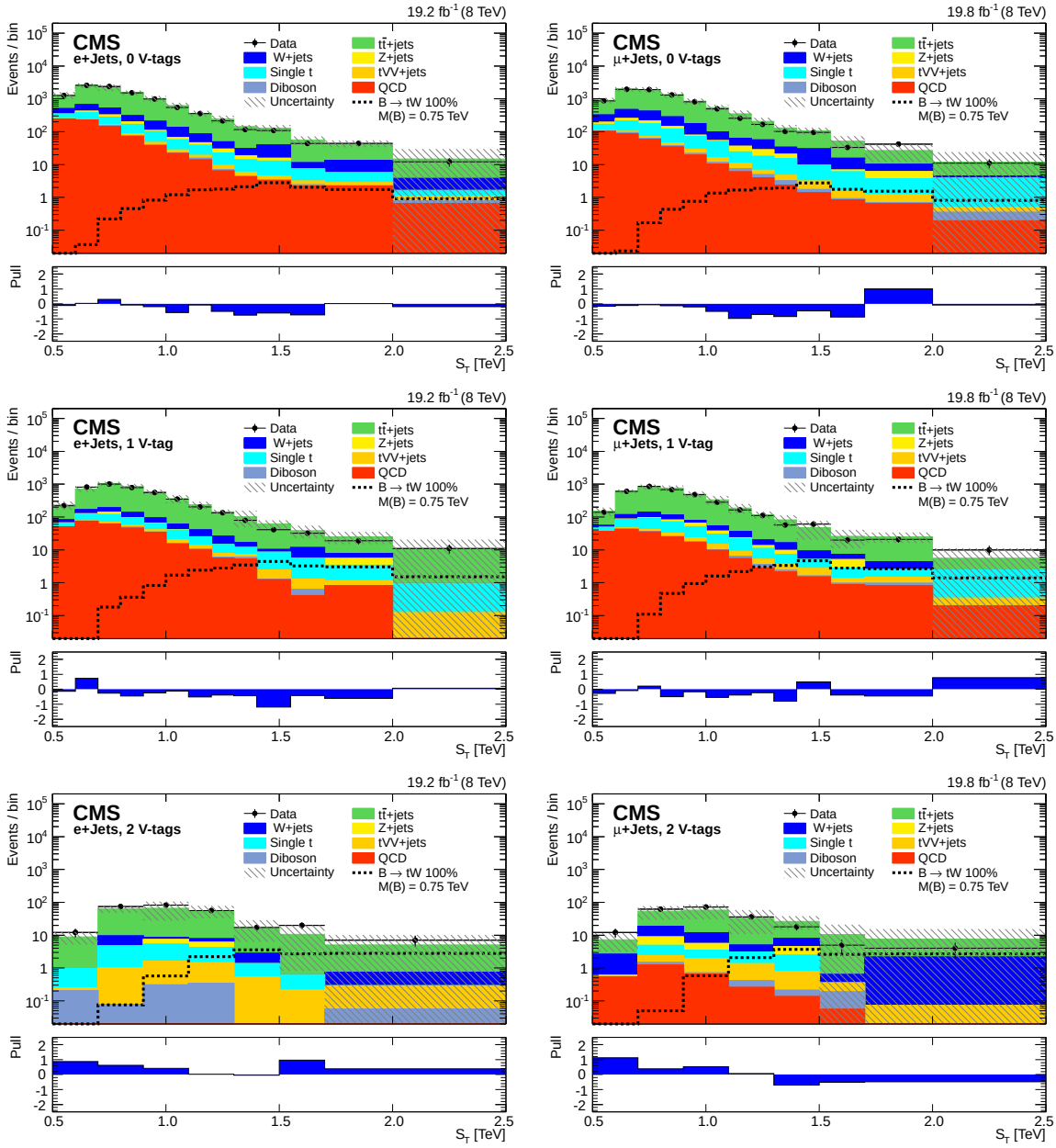

Figure 3: The S_T distributions in the 0, 1, and ≥ 2 V-tag categories in the electron+jets channel (left) and muon+jets channel (right). The uncertainty bands shown include statistical and all systematic uncertainties, added in quadrature for each single bin. The horizontal bars on the data points indicate the bin width. The difference between the observed and expected events divided by the total statistical and systematic uncertainty of the background prediction (pull) is shown for each bin in the lower panels.

having same-sign lepton pairs to the number of events having those of opposite sign. This contribution to the background model is then normalized by selecting opposite-sign lepton pairs in the signal region and multiplying by this charge misidentification rate.

Finally, there can be events passing the selection containing either one or two nonprompt leptons that pass the analysis lepton criteria. To estimate this background contribution a looser lepton selection is applied, where the isolation requirement is relaxed for electrons; the isolation, impact parameters, and track quality requirements are relaxed for muons. Leptons passing these relaxed criteria are known as "loose" leptons, while those passing the signal region selection are known as "tight" leptons. Using data events, misidentification rates for nonprompt leptons to be reconstructed as tight leptons are measured (f_i, where i is 1 for the leading and 2 for the subleading nonprompt lepton), along with the rates for prompt leptons to be reconstructed as tight leptons (p_i, where i is the index of the prompt lepton in this case). Using these loosened selection criteria, the expected yields for events containing 0, 1, or 2 nonprompt leptons (N_{ff}, $N_{pf/fp}$, N_{pp}, respectively, where the subscript f refers to misidentified leptons) can be computed by using the observed numbers of events containing 0, 1, or 2 loose leptons (N_{TT}, $N_{TL/LT}$, N_{LL}, respectively), according to the relation shown in Eq. (1):

$$\begin{pmatrix} N_{pp} & N_{pf} & N_{fp} & N_{ff} \end{pmatrix} = \begin{pmatrix} N_{LL} & N_{TL} & N_{LT} & N_{TT} \end{pmatrix} \times \begin{pmatrix} (1-p_1)(1-p_2) & p_1(1-p_2) & (1-p_1)p_2 & p_1p_2 \\ (1-p_1)(1-f_2) & p_1(1-f_2) & (1-p_1)f_2 & p_1f_2 \\ (1-f_1)(1-p_2) & f_1(1-p_2) & (1-f_1)p_2 & f_1p_2 \\ (1-f_1)(1-f_2) & f_1(1-f_2) & (1-f_1)f_2 & f_1f_2 \end{pmatrix}^{-1} . \quad (1)$$

After using this method to estimate the background from the contributions containing nonprompt leptons, the S_T distribution is used to discriminate signal events from background. The S_T distributions for the dielectron, dimuon, and electron-muon channels are shown in Fig. 4.

5.3 Opposite-sign lepton pair channel

The main background in the opposite-sign dilepton channel is from the inclusive Z+jets process (93%), with the remaining fraction due to $\mathrm{t\bar{t}}$+jets and diboson processes. Instead of using simulated events, control samples in data are used to predict the normalization and shape of the $M(\ell\ell\mathrm{b})$ spectrum of the background. The background is estimated from data using an $ABCD$ method to predict the bZ invariant mass distribution $M(\ell\ell\mathrm{b})$ in the signal region, labeled B, using control regions A, C, and D. The classification of the events into region A, B, C, or D is made using event selection variables that are largely uncorrelated for the background samples. The two variables chosen are the number of jets, N_{jets}, and the b-tagging discriminator of the highest p_T jet in the event. With an identified Z boson decaying leptonically, there will be at least two jets expected in signal events, providing discrimination power against SM background processes.

The selections used are (*i*) either $N_{\text{jets}} = 1$ or $N_{\text{jets}} > 1$ and (*ii*) events with the leading jet either passing or failing the b-tagging discriminator threshold (>0.679). These selections divide the N_{jets} vs. b-tagging discriminator plane into the four regions shown in Fig. 5. The signal contribution outside the signal region B was found to be negligible using simulated event samples. Under the hypothesis of complete noncorrelation between N_{jets} and the b-tagging discriminator, the number of background events in the signal region would be given by $N_B = N_A \times N_D / N_C$, where N_X is the number of events in the corresponding region. However, residual correlation between the two variables is present and must be taken into account

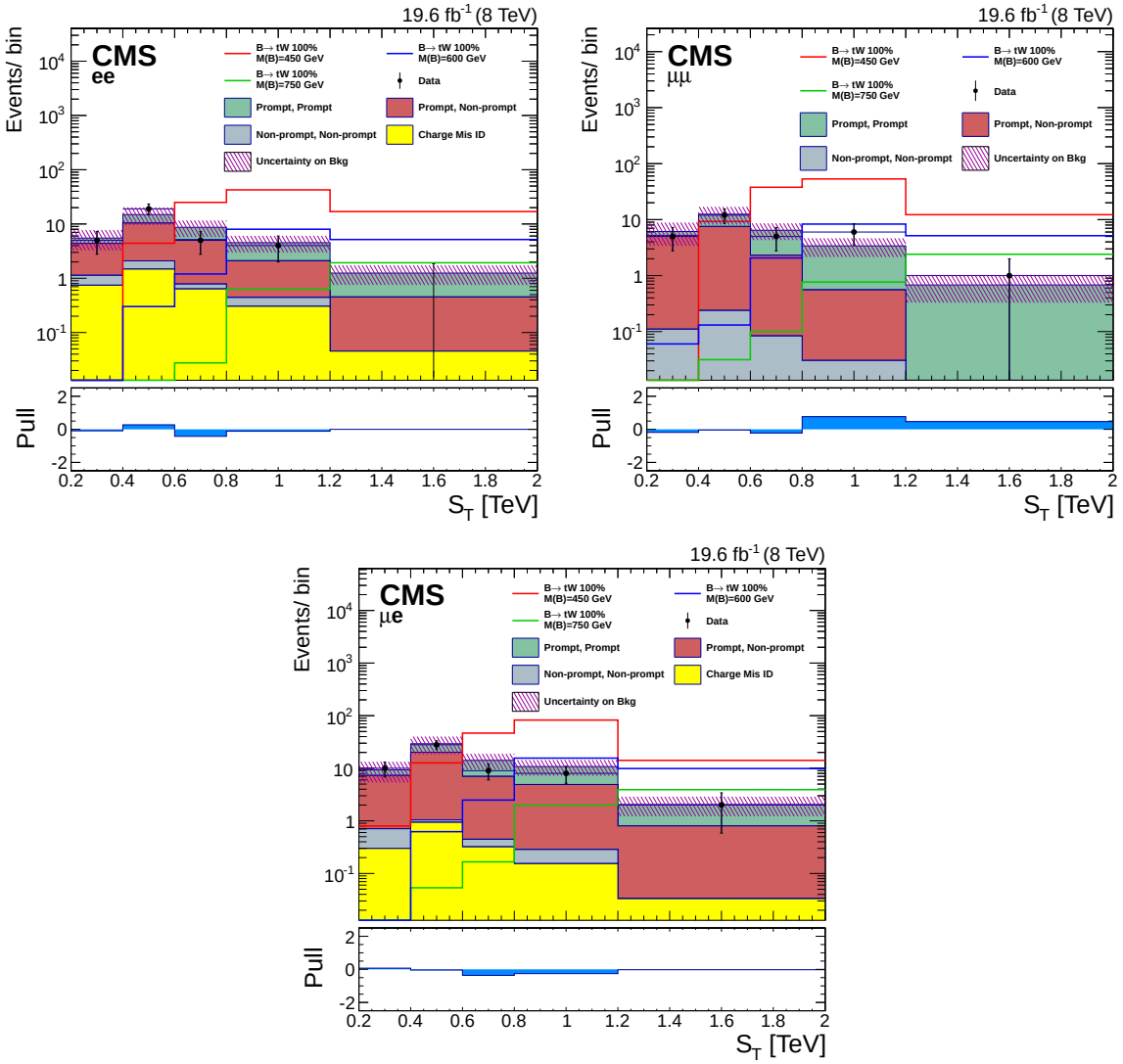

Figure 4: The S_T distributions used for signal discrimination in the same-sign dilepton channel. The distribution is shown for the three dilepton categories used: dielectron (top left), dimuon (top right), and electron-muon (bottom). The horizontal bars on the data points indicate the bin width. The difference between the observed and expected events divided by the total statistical and systematic uncertainty of the background prediction (pull) is shown for each bin in the lower panels.

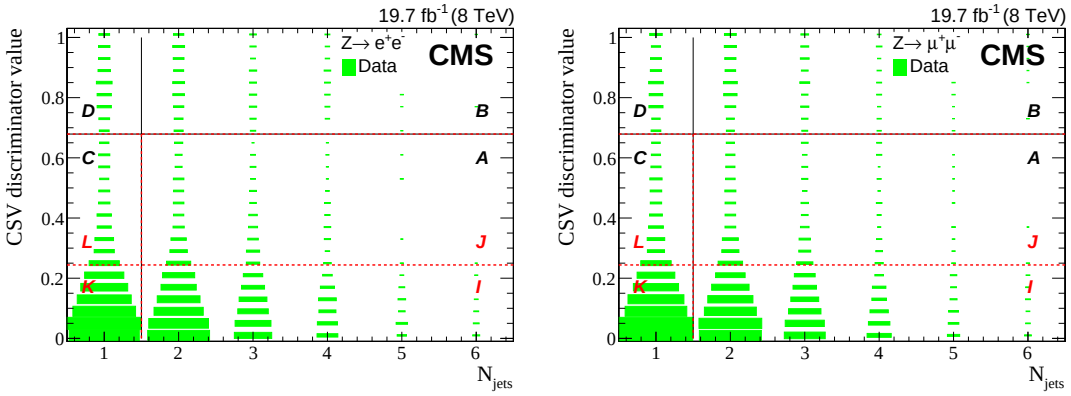

Figure 5: The event distribution in the plane of N_{jets} vs the b-tagging discriminator value, used to define the regions A, B, C, and D for the opposite-sign dilepton $\text{Z} \to \text{e}^+\text{e}^-$ (left) and $\text{Z} \to \mu^+\mu^-$ (right) channels. The region B is the signal region while the others constitute the control regions. The regions I, J, K, and L are used for estimation of systematic uncertainties. All other selection criteria used to select the B quark candidates have been applied. The area of each bar is proportional to the number of events in a given bin of the distribution of N_{jets} vs b-tagging discriminator.

in the background estimation procedure. The correlation is measured from data using an alternative set of control regions defined using the following criteria: (*i*) $N_{\text{jets}} = 1$ or $N_{\text{jets}} > 1$ and (*ii*) $0.244 <$ b-tagging discriminator < 0.679 or b-tagging discriminator < 0.244 for the leading jet. This classification divides the N_{jets} vs the b-tagging discriminator plane into four regions, labeled I, J, K, and L, as shown in Fig. 5. These four regions are completely contained within the previously defined regions A and C. The ratio $\mathcal{C} = N_J N_K / N_I N_L$ is equal to 1 if N_{jets} and the b-tagging discriminator variables are perfectly uncorrelated, and is used to quantify the degree of correlation between the two. The number of background events, taking into account the correlations, is given by $N_B\,\mathcal{C}$. The values of $\mathcal{C}$ were measured to be 1.29 ± 0.08 for $\text{Z} \to \text{e}^+\text{e}^-$ and 1.38 ± 0.07 for the $\text{Z} \to \mu^+\mu^-$ channels, where the uncertainties are statistical and related to the sample sizes in the regions I, J, K, and L. These factors are significantly different from unity, implying some degree of correlation between N_{jets} and the b-tagging discriminator. Closure tests were performed with simulated samples, as well as with data control samples with selections orthogonal to those for the regions described above. The values of the correlation factors obtained were consistent within uncertainties and stable with respect to the variation of the b-tagging discriminator values within $\pm 10\%$.

While the above procedure is used to predict the total number of background events, the shape of the $M(\ell\ell\text{b})$ background distribution is assumed to be the same in the signal region and the region A. This assumption is justified by examining the $M(\ell\ell\text{b})$ distributions in the signal region and in region A, using simulated events. The shapes obtained are consistent within the uncertainties in each. The total event yields in data and the estimated background are given in Table 3. The uncertainty in this background estimation is given by a combination of the statistical and systematic sources described in Sec. 6.

The expected yields for the signal with different B quark masses and two different values of the branching fraction, 100% and 50%, for $\text{B} \to \text{bZ}$ are given in Table 4. Since we require exactly one opposite-charge lepton pair, the probability of identifying a B quark does not depend on the decay of the other B quark. Figure 6 shows the mass spectra of the reconstructed B quark candidates, and the estimated background. The expected B quark signals, for $M(\text{B}) = 450$ and 700 GeV, are also shown. The error bars on the expected background are due to the statistical

Table 3: Expected background yields and observed number of events in data in the opposite-sign dilepton channel. The background is obtained from data. The background uncertainties include both statistical and systematic components.

	$Z \to e^+e^-$	$Z \to \mu^+\mu^-$
Expected background	379 ± 70	534 ± 79
Observed events	334	542

Table 4: Expected signal event yields in the opposite-sign dilepton channel, shown for B quark masses $M(B)$ from 450 to 800 GeV and for two values of the branching fraction.

	$\mathcal{B}(B \to bZ) = 100\%$		$\mathcal{B}(B \to bZ) = 50\%$	
$M(B)$ [GeV]	$Z \to e^+e^-$	$Z \to \mu^+\mu^-$	$Z \to e^+e^-$	$Z \to \mu^+\mu^-$
450	214±13	336±16	102±4	162±5
500	122±7	209±9	56±2	94±3
550	76±4	114±5	33±1	54±2
600	36±2	66±3	17.6±0.7	30.8±0.9
650	23±1	41±2	11.0±0.4	19.5±0.6
700	14.1±0.7	25.9±1.0	6.5±0.2	12.0±0.3
750	7.6±0.4	15.5±0.6	3.6±0.1	7.4±0.2
800	4.8±0.3	9.9±0.4	2.2±0.1	4.6±0.1

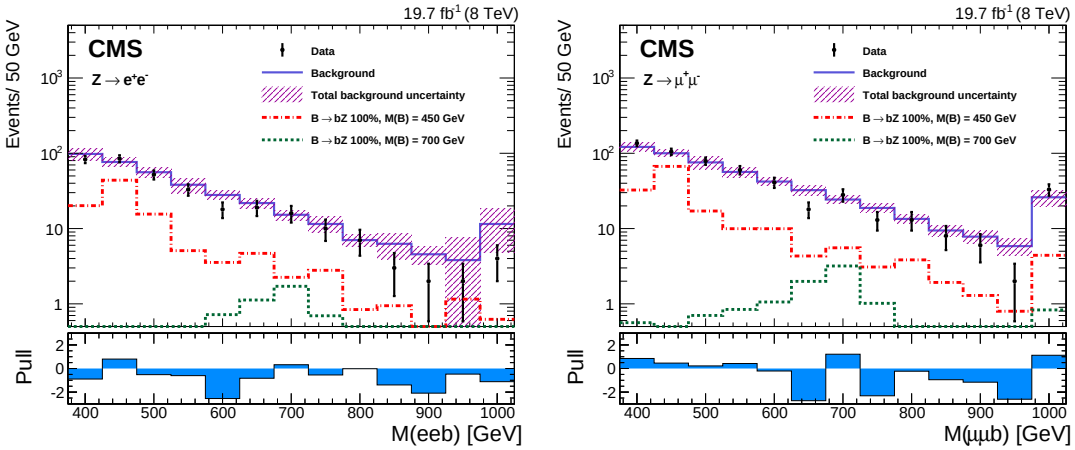

Figure 6: The invariant mass of reconstructed B quark candidates in the opposite-sign dilepton $Z \to e^+e^-$ (left) and $Z \to \mu^+\mu^-$ (right) channels. The estimated background is shown by the solid line, along with the total uncertainty (hatched area). The last bin of the histograms contains all events with $M(\ell\ell b) > 1000$ GeV. The signal contribution is shown for two B quark masses. The difference between the observed and expected events divided by the total statistical and systematic uncertainty of the background prediction (pull) is shown for each bin in the lower panels.

uncertainties as well as the uncertainty from the background estimation method. The overall normalization of the background agrees with the observed number of events. The $M(\ell\ell b)$ distributions in both the $Z \to e^+e^-$ and the $Z \to \mu^+\mu^-$ channels show some discrepancies between data and expectation in a few bins, caused by a flavor dependence in the reconstructed $M(\ell\ell j)$ distribution observed in Z+jets events. The control region A is more enriched in light quark flavors than the signal region B, leading to the observed discrepancy. A systematic uncertainty is applied to cover this effect, based on the shape differences observed between the

control regions I and J in data. In simulation, these regions were found to have relative flavor content similar to the regions A and B.

5.4 Multilepton channel

In multilepton channels, the level of the SM background contribution varies considerably across event categories. The categories with hadronic tau decays or OSSF lepton pairs suffer from larger background contributions than the others. Therefore, we improve sensitivity to new physics by separating categories with low and high background contributions. We categorize events with three leptons separately from those with four or more leptons. Events with identified b jets, having higher background from $\mathrm{t\bar{t}}$ events, are classified separately.

We consider backgrounds from rare processes such as $\mathrm{t\bar{t}W}$, $\mathrm{t\bar{t}Z}$, $\mathrm{t\bar{b}Z}$, where simulated events are used. The main SM background sources in multilepton+jet events include dilepton processes such as Z+jets, VV+jets, and $\mathrm{t\bar{t}}$+jets production with a misidentified lepton that passes selection criteria, and processes containing two leptons and an additional off-shell photon that undergoes a conversion, giving another reconstructed lepton. The above backgrounds are estimated using simulated events, except for the Z+jets and $\mathrm{W^+W^-}$+jets backgrounds, which are estimated from data, as described below.

Backgrounds from $\mathrm{t\bar{t}}$ enriched processes are estimated from simulation, after validation in single-lepton and dilepton control regions. In the single-lepton control region, exactly one isolated muon with $p_{\mathrm{T}} \geq 30\,\mathrm{GeV}$, at least three jets (one of which is b tagged), and $S_{\mathrm{T}} \geq 300\,\mathrm{GeV}$ are required. The dilepton control region requires an eμ combination and is used to compare kinematic variables such as S_{T} (see Fig. 7), H_{T}, and $\not\!\!E_{\mathrm{T}}$ between data and simulation. In this channel, H_{T} is defined as the scalar sum of selected jet p_{T} values. Additionally, the distribution of the number of jets is reweighted to match data for both the single-lepton and dilepton control regions.

Standard model WZ+jets and ZZ+jets production where both bosons decay leptonically can produce three prompt and isolated leptons with large H_{T} and $\not\!\!E_{\mathrm{T}}$. This class of background is irreducible since its final state cannot be distinguished from the signal scenario. Simulated events are used to model this background contribution. We scale the simulation to match the measured lepton efficiencies and $\not\!\!E_{\mathrm{T}}$ resolution. We verify the simulation by comparing to a data sample enriched in WZ production, the dominant contribution to trilepton signatures from VV+jets. The WZ events are selected by requiring three leptons, $50 < \not\!\!E_{\mathrm{T}} < 100\,\mathrm{GeV}$, a Z boson candidate with $M(\ell^+\ell^-)$ in the range 75–105 GeV, and $H_{\mathrm{T}} < 200\,\mathrm{GeV}$. We apply a constant scale factor of 1.14 to the WZ simulation, chosen to normalize the simulation to data in the region $50 < \not\!\!E_{\mathrm{T}} < 100\,\mathrm{GeV}$ for the observed transverse mass of the W boson, shown in Fig. 7.

Off-shell photon conversions can produce a lepton with very low p_{T} that will not pass the selection criteria or will not be reconstructed. Drell-Yan processes with such conversions can lead to a significant background for the three-lepton category. A measurement of the extrapolation factors for photon conversions to electrons or muons is performed using data events. We measure the extrapolation factors in a control region devoid of signal events, with low H_{T} and $\not\!\!E_{\mathrm{T}}$. The ratio of the number of events with $|M(\ell^+\ell^-\ell'^{\pm}) - M(\mathrm{Z})| < 15\,\mathrm{GeV}$ or $|M(\ell^+\ell^-\ell^{\pm}) - M(\mathrm{Z})| < 15\,\mathrm{GeV}$ to the number of events with $|M(\ell^+\ell^-\gamma) - M(\mathrm{Z})| < 15\,\mathrm{GeV}$ defines the extrapolation factor, which is $2.1 \pm 0.3\%$ ($0.7 \pm 0.1\%$) for electrons (muons). The measured extrapolation factors are then used to estimate the background in the signal region from the observed number of $\ell^+\ell^-\gamma$ events in the search region. The lepton selections of this channel strongly reject external conversions, where an on-shell photon converts to an $\ell^+\ell^-$ pair in the material of the detector.

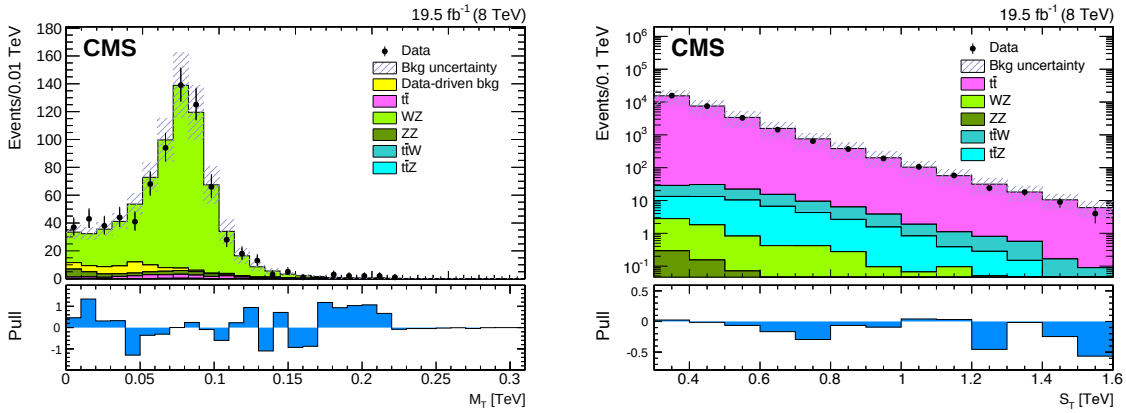

Figure 7: The transverse mass M_T distribution of events in a control sample of the multilepton analysis, enriched in WZ by requiring an OSSF pair with $M(\ell\ell)$ in the Z boson mass window and $50 < \not{E}_T < 100\,\text{GeV}$ (left). The S_T distribution for events containing an opposite-sign eμ pair in the $t\bar{t}$ control region of the multilepton analysis (right). Uncertainties include both statistical and systematic contributions. The difference between the observed and expected events divided by the total statistical and systematic uncertainty of the background prediction (pull) is shown for each bin in the lower panels.

We use data to estimate background contributions from processes with two genuine leptons and one or more misidentified leptons such as $Z(\ell\ell)$+jets and $W^+W^-(\ell\ell + \not{E}_T)$+jets. In order to estimate background from jets producing misidentified light-lepton candidates that appear to be prompt and isolated, we use data events containing two reconstructed leptons and an additional isolated track. This contribution is then scaled by an extrapolation factor relating isolated tracks to lepton candidates from jets. This light-lepton extrapolation factor is measured in control samples where no signal is expected, such as in the low-$\not{E}_T$ or low-H_T regions. We measure the extrapolation factor between isolated tracks and electron (muon) candidates to be $0.7 \pm 0.2\%$ $(0.6 \pm 0.2\%)$, using a data sample dominated by Z+jets. The contribution from backgrounds containing a misidentified third lepton is determined by multiplying the number of events containing isolated tracks in the sample with two leptons by the light-lepton extrapolation factor. Similarly, we estimate misidentified background contributions for the four-lepton selection by examining two-lepton events with two additional isolated tracks. Since the light-lepton misidentification rates vary with the b quark content across the control samples, the rate is determined as a function of the impact parameter distribution of nonisolated tracks in data.

Unlike electrons and muons, hadronically decaying tau leptons cannot be easily identified without an isolation requirement. Therefore, the dominant background in tau identification is from jets reconstructed as τ_h candidates. To measure this contribution, we loosen the isolation requirements on reconstructed tau leptons to get an extrapolation factor between nonisolated taus and isolated taus. We extrapolate the sideband region, $6 < I < 15\,\text{GeV}$, to a signal region, $I < 2\,\text{GeV}$, where I is defined as the amount of energy reconstructed in a cone of $\Delta R < 0.3$ around the tau lepton candidate, excluding the tau lepton candidate itself. We measure the extrapolation factor for jets reconstructed as taus, defined as the ratio of the number of tau candidates in the signal region to the number in the sideband region, to be $20 \pm 6\%$. The ratio is applied to a selection of events in a sideband region containing two light leptons and a tau lepton to estimate the contribution from misidentified τ_h candidates.

Events are divided into categories based on the reconstructed objects, using the background estimates described above. These categories include the number of identified leptons, number of identified tau leptons, number of b-tagged jets, and number of Z bosons reconstructed with

an OSSF lepton pair. Figure 8 shows the S_T distribution for two of these event categories. To further discriminate the B quark signal from SM background events, the S_T distribution is divided into several individual bins: 0–0.3, 0.3–0.6, 0.6–1.0, 1.0–1.5, 1.5–2.0, and >2.0 TeV. These bins are chosen such that the SM backgrounds fall mainly in the lowest two S_T bins, while the signal events occupy the higher S_T bins. Each of these bins is used as the basis for a counting experiment in the final analysis; no further shape discrimination is used within an individual S_T bin.

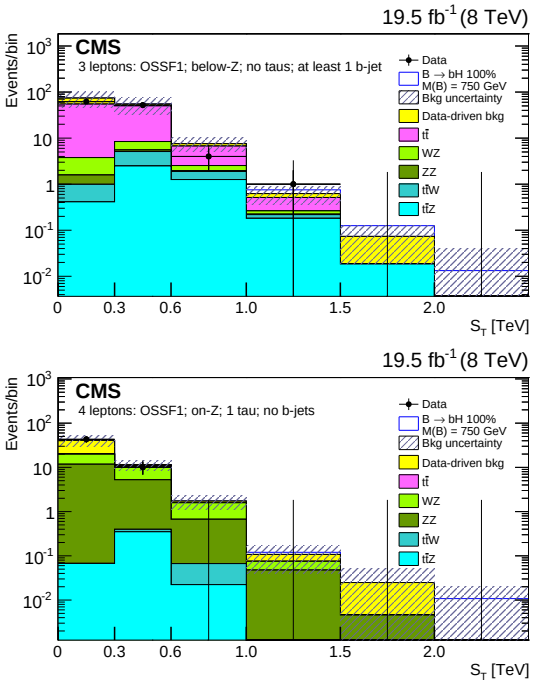

Figure 8: Distributions of S_T for two event categorizations in the multilepton channel: (top) three leptons, no tau leptons, at least one b-tagged jet, and no reconstructed Z boson candidate; (bottom) four leptons, one tau lepton, no b-tagged jets, and one reconstructed Z boson candidate. Uncertainties include both statistical and systematic contributions. The data-driven contribution includes contributions from two genuine leptons and one or more misidentified leptons. The horizontal bars on the data points indicate the bin width.

5.5 All-hadronic channel

The dominant background for the all-hadronic channel comes from SM multijet production. The smaller $t\bar{t}$+jets background is obtained from simulation, with corrections to account for differences between data and simulation. The nontop multijet background is obtained from the data. For the multijet background, an *ABCD* method is used to categorize events into four different categories.

First, events are sorted into categories with H-tagged jets or "anti-H-tagged" jets. Events may contain H-tagged jets, as described in Sec. 4.5. For events not containing H-tagged jets, the criteria of anti-H-tagged jets are defined as follows. Pruned CA8 jets are selected such that both the pruned subjets have the b-tagging discriminator variable between 0.244 and 0.679. All other criteria are the same as those for the H-tagged jets. This sideband of the b-tagging discriminator variable selects jets enriched in backgrounds with a negligible contribution from signal events.

Next, the pruned mass of the leading H-tagged jet or anti-H-tagged jet defines the second

selection. Higgs boson candidates, i.e., H-tagged jets with $90 < M_{\text{pruned}} < 140\,\text{GeV}$ form the first category of events. This is the signal region, labeled as B. Events with $M_{\text{pruned}} < 80\,\text{GeV}$ form the second category, labeled as A. Likewise anti-H-tagged events are categorized into the C and D categories depending on whether the leading anti-H-tagged jet satisfies $90 < M_{\text{pruned}} < 140\,\text{GeV}$ or $M_{\text{pruned}} < 80\,\text{GeV}$, respectively.

Since the event classification variables are uncorrelated, the relation $N_B = N_A\,N_C/N_D$ gives the background yields N_B in the signal region B based on the yields $N_{A,C,D}$ in the sideband regions A, C, or D, respectively.

Closure tests of the background estimation method were performed separately using simulation and data, with a control sample consisting of events with no b jets. For the b-jet veto, events with AK5 jets with $p_{\text{T}} > 30\,\text{GeV}$ and having a b-tagging discriminant value greater than 0.244 are rejected. The b-jet veto criteria applied are stricter than the selection criteria of b jets used for selecting signal events, thus the control sample is orthogonal to the signal sample. In this case, the region B still contains Higgs candidates and the rest of the sidebands A, C, and D are as defined above, but without any b jet.

In the b-jet-vetoed sample, two separate event categories are defined: one with exactly one AK5 jet with $p_{\text{T}} > 80\,\text{GeV}$, and the other with $\geq$2 AK5 jets with $p_{\text{T}} > 80\,\text{GeV}$. In both the simulated sample and in the data, the estimated and actual numbers of background events in the signal region B are found to be in agreement. Furthermore, the distributions of H_{T} for the predicted and the actual background are consistent within measurement uncertainties. The predicted and actual background yields in the data control sample are given in Table 5, while the agreement in the predicted and actual background H_{T} distributions is shown in Fig. 9.

Table 5: Closure test of the background estimation method for the all-hadronic channel, in the data using a control sample with no b jets. The background is estimated from the sideband regions A, C, and D. The product $N_A\,(N_C/N_D)$ is compared with the actual background observed in region B in the data. The uncertainties correspond to the statistical uncertainties from limited sample sizes. The agreement obtained is within the uncertainties.

	Yields in 1 jet category	Yields in $\geq$2 jet category
Background estimation	2059 ± 70	2456 ± 79
True background	2087	2449

After closure tests are performed, the $ABCD$ background estimation method is applied to the signal region, and the estimated backgrounds in the 1 b jet, the $\geq$2 b jets, and combined categories are shown in Table 6. The background estimated in this way is in agreement with the observed number of events. The H_{T} distributions in the categories with 1 and $\geq$2 b jets are shown in Fig. 10 and show agreement in both shape and normalization with the observed H_{T} distributions. The uncertainty in the background estimation is propagated from the statistical uncertainties of the samples in the sideband regions and also includes the statistical uncertainties in the control samples. No additional systematic uncertainty has been assigned. Upper limits on the $\text{B}\overline{\text{B}}$ cross section are derived using these distributions.

6 Systematic uncertainties

Several sources of systematic uncertainty are considered when testing for the presence of B quark signal events. These uncertainties include those associated with detector measurements such as jet and lepton reconstruction and the luminosity determination, as well as theoretical uncertainties in the cross section due to the choice of renormalization and factorization scales.

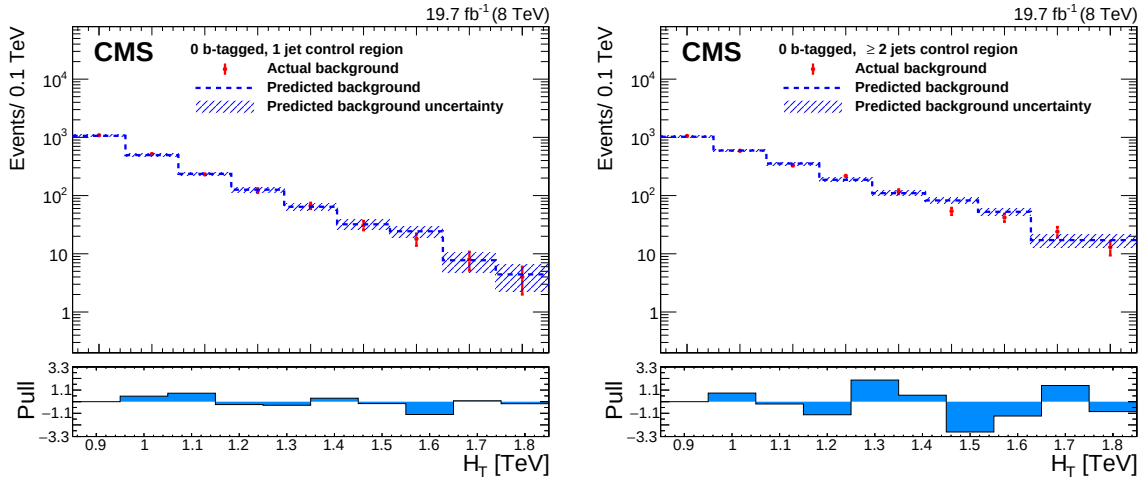

Figure 9: Background closure test in the data control samples of the all-hadronic analysis with no b jets and exactly one AK5 jet with $p_T > 80$ GeV (left) and with $\geq$2 AK5 jets with $p_T > 80$ GeV (right). The red data points represent the actual background as derived from data. The blue dashed line represents the predicted background, with the hatched area depicting the corresponding uncertainty. The difference between the observed and predicted background divided by the total uncertainty in the background prediction (pull) is shown for each bin in the lower panels.

Table 6: Estimated background and the event yields in the data for the 1 b jet, $\geq$2 b jets, and combined event categories in the all-hadronic channel. The uncertainties in the background yields are obtained by propagating the statistical uncertainties from the sideband samples.

	Yields after full selection	Yields in 1 b-tagged category	Yields in $\geq$2 b-tagged category
Estimated background	872^{+49}_{-55}	825^{+47}_{-52}	46^{+4}_{-11}
Data	903	860	43

Finally, there are uncertainties specific to individual analyses, such as those arising from background estimation methods using data. In this section we detail the sources of systematic uncertainty affecting the various analyses of individual channels of which the results are then combined for the overall result. Table 7 summarizes these sources.

The jet energy scale and the jet energy resolution uncertainties are taken as fully correlated between each of the individual channels. These uncertainties are associated with the calibration of the jet energy response in the detector readout. This calibration procedure, which is dependent on jet p_T and pseudorapidity, leads to an approximately 10% uncertainty in the normalization of event yields. This uncertainty is applied on an event-by-event basis, resulting in an additional shape effect. As we observe a difference between the simulated jet energy resolution and the jet energy resolution measured in data, we smear the jet energies in simulation to reflect the energy resolution observed in data. This procedure introduces a small uncertainty in the shape of jet kinematic properties in simulated events, including a normalization effect of less than 5%.

In addition to the uncertainty in the measurement of integrated luminosity of 2.6% [58], several scale factors (SF) are applied to simulated events to reflect the differences with data in reconstruction efficiencies for various objects used in the event selections. The uncertainties in these SF measurements are applied to the relevant events. These uncertainties vary for individual

Table 7: Nuisance parameters applied to the statistical combination. They are listed separately for each individual channel, and the ✓ symbol is used if they are applied to that given channel. If a nuisance parameter is taken as correlated between channels, the ☑ symbol is shown. In some cases, several systematic uncertainties are combined into a single nuisance parameter (for example, in the case of combined lepton categories); in such instances, the • symbol is used to denote the presence of a systematic uncertainty combined with others in a distinct nuisance parameter. The $\sim$ symbol has been used to denote systematic uncertainties that have negligible effects on the analysis results. The "Combined systematic uncertainty" entry represents a contribution composed of other sources listed in the table, applied as a single nuisance parameter during limit extraction.

	Lepton+jets	OS dilepton	SS dilepton	Multilepton	All hadronic
Jet energy scale	☑	☑	☑	☑	☑
Jet energy resolution	☑	☑	☑	$\sim$	☑
V-tag SF	✓				✓
$t\bar{t}$ matching scale	✓				•
$t\bar{t}$ renormalization/factorization scales	✓				•
b-tagging SF	☑	•		☑	•
Light-jet-tagging SF		•			•
Integrated luminosity	☑	☑	☑	☑	☑
Lepton reconstruction	✓	✓	✓	•	
$t\bar{t}$ cross section	☑			☑	
QCD normalization	✓				
Trigger efficiency	✓	✓	✓	•	✓
Pileup uncertainty	$\sim$	☑	☑	$\sim$	☑
Background component from data		✓	✓	•	
PDF uncertainty	$\sim$	$\sim$	✓	•	✓
$\not{E}_T$ resolution				✓	
Initial-state radiation				✓	
Combined systematic uncertainty	✓		✓	✓	✓

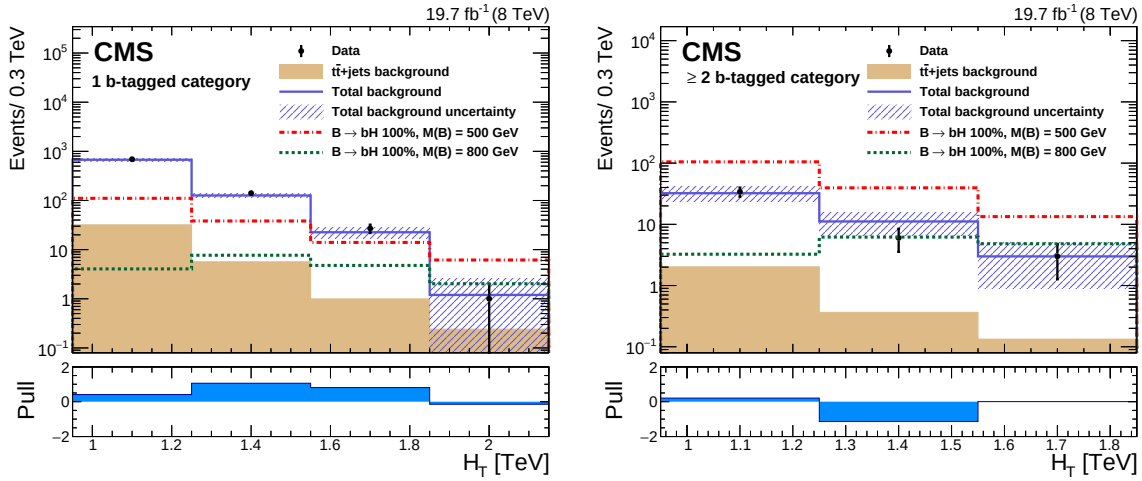

Figure 10: The H_T distributions in the 1 b jet (left) and the $\geq$ 2 b jets event categories (right) for the all-hadronic analysis. The blue solid line depicts the estimated background, with the hatched area showing the measured uncertainty in the background. The signal contributions for two B quark mass points, 500 and 800 GeV, are overlaid. The bin width is chosen to have a statistically significant number of events in every bin. The difference between the data and the estimated background divided by the total uncertainty in the background (pull) is shown for each bin in the lower panels.

channels, but they include SF uncertainties for the electron and muon identification and efficiency values, typically 1%-2%, as well as SF uncertainties for the b-tagging algorithms used, at approximately 5%, and finally specific SF uncertainties for the identification of hadronically decaying high-p_T W, Z, or Higgs bosons, which can be up to 10% depending on the algorithm used, resulting from the number of events used to measure the appropriate SFs.

For simulated $t\bar{t}$ events, several specific systematic uncertainties are applied to cover differences in generation parameters. The renormalization and factorization scales are varied up and down coherently by a factor of 2 to produce a shape uncertainty for the simulated $t\bar{t}$ events. This shape template has a normalization effect of roughly 20%, in addition to the shape component. The scale used for the parton matching in PYTHIA is changed to measure an additional systematic uncertainty. This component is smaller, and is about a 10% effect. Finally, an uncertainty of 15% is applied resulting from the measurement of the $t\bar{t}$ cross section [59]. This is applied as purely a normalization effect. These uncertainties only apply to simulated $t\bar{t}$ events.

We also include systematic uncertainties associated with the choice of the CTEQ6L1 PDF set. These are estimated by applying weighting factors to vary the elements of the eigenvector used in the PDF simulation. The weights are combined in quadrature to compute a total systematic uncertainty in the shape and normalization of simulated $t\bar{t}$ and signal events due to PDF effects.

Finally, there are several uncertainties specific to individual channels. In some cases, all relevant uncertainties are combined into a single nuisance parameter affecting the normalization, for example for the multilepton channels, which include several counting experiments without shape effects. Other uncertainties include those for background estimates from data, and are detailed in the corresponding previous sections.

For the statistical combination, we correlate the systematic uncertainties that arise from the same physical effect or phenomenon, such as the jet energy scale, luminosity measurement, or $t\bar{t}$ cross section. These correlations allow us to better constrain the uncertainties by using inde-

pendent information from various channels. This procedure further improves the sensitivity of the combination.

7 Combination strategy

Each of the five channels has a distinct method to discriminate the B quark signal from the expected background contribution. In the case of the lepton+jets channel, the S_T distribution is used (Fig. 3), with different categories corresponding to unique numbers of merged vector bosons reconstructed in the final state. For the opposite-sign dilepton channel, the B quark candidate mass is reconstructed, and its distribution is used to discriminate the signal (Fig. 6). In the case of the same-sign dilepton and multilepton channels, for each of the various event categorizations, the S_T variable is used for signal discrimination, and each bin of the S_T distribution (Figs. 4 and 8) is treated as an independent counting experiment. The results are combined to produce a cross section limit. Finally, the all-hadronic channel uses the H_T distribution separately for single- and double-b-tagged events (Fig. 10).

We combine all signal bins of the five individual analysis channels for the result. A joint likelihood maximization is performed, simultaneously using the background and signal expectations in each bin, to extract the final results using a Bayesian approach. We scan over the entire parameter space of the B quark branching fractions in steps of 0.1 for each possible B quark decay mode.

Nuisance parameters are included in the joint likelihood maximization to account for the various systematic uncertainties described above. For those uncertainties that arise from the same physical or detector effect and are shared between individual channels, the corresponding nuisance parameters are taken to be 100% correlated in the fitting procedure. All nuisance parameters describing systematic uncertainties are implemented either with Gaussian priors (for normalization effects) or through template interpolation (for shape changing effects). The parameter governing the signal normalization is implemented with a uniform prior distribution.

No significant excess above SM expectations is observed. We set limits on the $B\overline{B}$ production cross section using the combination of all individual channels to further improve the sensitivity to this process.

8 Results

Since the vectorlike B quark can decay in three possible topologies (tW, bZ, and bH), we scan over the entire possible parameter space of decays, using steps of 10% in each branching fraction. This results in 66 combinations of branching fractions, each with its own cross section limits as a function of the B quark mass. The results are shown in the form of limits on the B quark pair-production cross section and are quoted at 95% CL.

The various channels have targeted different final-state topologies, and thus they will contribute to separate regions of the parameter space of decay possibilities. For example, the lepton+jets channel is sensitive to the tW decay mode but is less sensitive to bH and bZ final states. The opposite-sign dilepton channel is sensitive to the bZ decay but less so to bH or tW. The relative contributions of each channel in the case of a 100% branching fraction for a specific decay mode are shown in Fig. 11. In some cases, a channel does not have sensitivity to a certain decay topology and is not included at all in the corresponding result.

The expected and observed exclusion limits for the B quark are determined for each one of

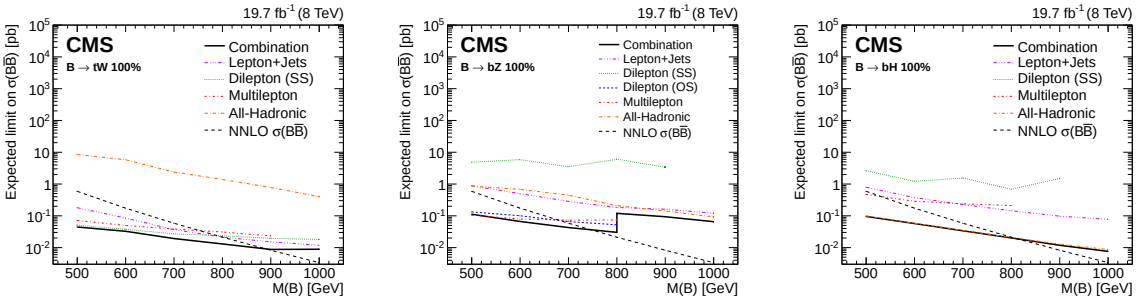

Figure 11: Comparison of individual channel limit results with those of the combination, for the expected limits only. Shown are the limit results, at 95% CL, for the three corners of the triangular parameter space, for 100% branching fractions for B to tW (left), bZ (middle), and bH (right). The same-sign and opposite-sign channels are denoted by "SS" and "OS", respectively. The step observed in the bZ limit curve is due to two analysis channels (multilepton and OS dilepton) that do not contribute to the combination for B quark masses above 800 GeV.

the 66 combinations of branching fractions. To visualize these results, we plot the B quark mass exclusion limits on a triangular parameter space, as shown in Fig. 12. We also list the cross section limits for different branching fractions and B quark masses in Table 8. Further details, including event yields for the various channels entering the combination, are available on HepData [60].

The expected and observed limits agree within the uncertainties. For the branching fraction B $\to$ tW of 100%, we expect to exclude $M(\mathrm{B}) < 890$ GeV and observe an exclusion of $M(\mathrm{B}) < 880$ GeV. This is the combination with the best sensitivity to B pair production. The remaining results are summarized in Table 9. Finally, the cross section limits as a function of B mass are shown graphically in Fig. 13 for the exclusive decay modes to tW, bZ, and bH. The multilepton and OS dilepton channels do not contribute to the combination for B quark masses above 800 GeV. This restriction does not affect the mass exclusion limits obtained from the combined result.

9 Summary

A search for pair production of the B quark with vectorlike couplings to W, Z, and Higgs bosons has been performed, using data recorded by the CMS experiment from proton-proton collisions at a center-of-mass energy of 8 TeV at the CERN LHC in 2012. This hypothesized particle could decay in one of three ways: to tW, bZ, or bH. The search is performed using five distinct topologies to maintain sensitivity to each of these decay modes. The topologies included in this search are the lepton+jets final state, both the opposite-sign and same-sign lepton pair final states, the three or more leptons final state, and finally the all-hadronic final state targeting Higgs boson decays to pairs of bottom quarks.

No evidence for the production of B quarks in any topology is found, and limits are set on the B quark-antiquark pair-production cross section. A scan over possible combinations of the branching fractions to tW, bZ, and bH is performed. For a B quark decaying with a branching fraction of 100% to bH, B quarks with masses up to 900 GeV are excluded, at 95% confidence level. This branching fraction corresponds to the highest excluded B quark mass in this scan. Observed exclusion limit results from a scan of all possible branching fractions range from a minimum of 740 GeV to 900 GeV. The combination of these results provides the most stringent exclusion limit to date for the existence of a vectorlike B quark.

Table 8: Cross section limits for various combinations of branching fractions and B quark masses. The expected cross section limits are given in the first row for each branching fraction combination, along with their corresponding uncertainties. The observed cross section limits are shown in the second row. All limits are given at 95% CL, and are shown in units of pb.

$\mathcal{B}$	$\mathcal{B}$	$\mathcal{B}$	B quark mass [GeV]					
(tW)	(bH)	(bZ)	500	600	700	800	900	1000
0.0	0.0	1.0	$0.112^{+0.089}_{-0.042}$	$0.066^{+0.041}_{-0.027}$	$0.043^{+0.027}_{-0.016}$	$0.030^{+0.020}_{-0.011}$	$0.094^{+0.053}_{-0.036}$	$0.065^{+0.036}_{-0.023}$
			0.090	0.037	0.036	0.029	0.096	0.083
0.0	0.2	0.8	$0.261^{+0.130}_{-0.115}$	$0.097^{+0.060}_{-0.043}$	$0.053^{+0.034}_{-0.025}$	$0.033^{+0.023}_{-0.014}$	$0.044^{+0.030}_{-0.016}$	$0.032^{+0.020}_{-0.012}$
			0.215	0.046	0.038	0.023	0.044	0.033
0.0	0.4	0.6	$0.267^{+0.138}_{-0.114}$	$0.107^{+0.065}_{-0.050}$	$0.052^{+0.034}_{-0.025}$	$0.030^{+0.022}_{-0.015}$	$0.028^{+0.020}_{-0.011}$	$0.020^{+0.012}_{-0.008}$
			0.210	0.065	0.037	0.020	0.027	0.021
0.0	0.6	0.4	$0.286^{+0.141}_{-0.141}$	$0.107^{+0.067}_{-0.054}$	$0.047^{+0.035}_{-0.024}$	$0.026^{+0.023}_{-0.013}$	$0.020^{+0.013}_{-0.009}$	$0.014^{+0.009}_{-0.006}$
			0.219	0.058	0.031	0.016	0.019	0.014
0.0	0.8	0.2	$0.268^{+0.145}_{-0.146}$	$0.101^{+0.070}_{-0.056}$	$0.045^{+0.031}_{-0.024}$	$0.022^{+0.014}_{-0.012}$	$0.016^{+0.010}_{-0.007}$	$0.011^{+0.008}_{-0.004}$
			0.131	0.061	0.030	0.016	0.014	0.010
0.0	1.0	0.0	$0.096^{+0.054}_{-0.037}$	$0.057^{+0.029}_{-0.023}$	$0.034^{+0.021}_{-0.015}$	$0.020^{+0.014}_{-0.009}$	$0.012^{+0.008}_{-0.005}$	$0.008^{+0.007}_{-0.003}$
			0.066	0.035	0.021	0.014	0.008	0.006
0.2	0.0	0.8	$0.183^{+0.095}_{-0.084}$	$0.073^{+0.049}_{-0.027}$	$0.040^{+0.028}_{-0.016}$	$0.028^{+0.018}_{-0.011}$	$0.046^{+0.022}_{-0.015}$	$0.036^{+0.015}_{-0.013}$
			0.140	0.041	0.033	0.029	0.058	0.046
0.2	0.2	0.6	$0.226^{+0.149}_{-0.101}$	$0.087^{+0.067}_{-0.037}$	$0.049^{+0.034}_{-0.020}$	$0.032^{+0.023}_{-0.013}$	$0.033^{+0.017}_{-0.013}$	$0.024^{+0.012}_{-0.009}$
			0.099	0.057	0.035	0.028	0.045	0.031
0.2	0.4	0.4	$0.275^{+0.123}_{-0.125}$	$0.097^{+0.061}_{-0.044}$	$0.048^{+0.036}_{-0.023}$	$0.027^{+0.022}_{-0.011}$	$0.024^{+0.014}_{-0.010}$	$0.018^{+0.010}_{-0.007}$
			0.131	0.049	0.032	0.021	0.027	0.022
0.2	0.6	0.2	$0.296^{+0.145}_{-0.131}$	$0.091^{+0.064}_{-0.045}$	$0.044^{+0.033}_{-0.022}$	$0.025^{+0.018}_{-0.012}$	$0.019^{+0.011}_{-0.008}$	$0.014^{+0.007}_{-0.005}$
			0.162	0.047	0.031	0.019	0.021	0.015
0.2	0.8	0.0	$0.267^{+0.151}_{-0.139}$	$0.084^{+0.064}_{-0.045}$	$0.040^{+0.028}_{-0.019}$	$0.022^{+0.017}_{-0.010}$	$0.015^{+0.010}_{-0.006}$	$0.010^{+0.007}_{-0.004}$
			0.107	0.052	0.023	0.018	0.015	0.012
0.4	0.0	0.6	$0.205^{+0.118}_{-0.091}$	$0.071^{+0.045}_{-0.028}$	$0.035^{+0.025}_{-0.014}$	$0.023^{+0.014}_{-0.009}$	$0.028^{+0.015}_{-0.009}$	$0.022^{+0.011}_{-0.007}$
			0.152	0.042	0.029	0.023	0.040	0.030
0.4	0.2	0.4	$0.218^{+0.122}_{-0.094}$	$0.079^{+0.046}_{-0.032}$	$0.039^{+0.030}_{-0.015}$	$0.026^{+0.017}_{-0.010}$	$0.023^{+0.011}_{-0.008}$	$0.018^{+0.009}_{-0.006}$
			0.111	0.047	0.027	0.025	0.032	0.026
0.4	0.4	0.2	$0.258^{+0.122}_{-0.105}$	$0.086^{+0.046}_{-0.038}$	$0.040^{+0.027}_{-0.019}$	$0.023^{+0.016}_{-0.010}$	$0.019^{+0.010}_{-0.006}$	$0.015^{+0.007}_{-0.005}$
			0.142	0.040	0.028	0.023	0.026	0.020
0.4	0.6	0.0	$0.235^{+0.111}_{-0.102}$	$0.087^{+0.052}_{-0.040}$	$0.038^{+0.026}_{-0.018}$	$0.023^{+0.015}_{-0.010}$	$0.016^{+0.008}_{-0.006}$	$0.012^{+0.006}_{-0.004}$
			0.139	0.043	0.028	0.015	0.020	0.015
0.6	0.0	0.4	$0.235^{+0.092}_{-0.097}$	$0.068^{+0.039}_{-0.030}$	$0.034^{+0.022}_{-0.014}$	$0.019^{+0.011}_{-0.008}$	$0.019^{+0.010}_{-0.006}$	$0.016^{+0.007}_{-0.005}$
			0.135	0.051	0.025	0.018	0.029	0.021
0.6	0.2	0.2	$0.241^{+0.097}_{-0.095}$	$0.067^{+0.045}_{-0.028}$	$0.033^{+0.024}_{-0.015}$	$0.019^{+0.013}_{-0.007}$	$0.017^{+0.008}_{-0.006}$	$0.014^{+0.006}_{-0.005}$
			0.163	0.035	0.022	0.015	0.024	0.020
0.6	0.4	0.0	$0.176^{+0.111}_{-0.079}$	$0.064^{+0.051}_{-0.025}$	$0.034^{+0.026}_{-0.015}$	$0.019^{+0.012}_{-0.008}$	$0.015^{+0.008}_{-0.005}$	$0.012^{+0.006}_{-0.004}$
			0.113	0.033	0.023	0.016	0.021	0.015
0.8	0.0	0.2	$0.209^{+0.091}_{-0.095}$	$0.057^{+0.030}_{-0.022}$	$0.027^{+0.019}_{-0.011}$	$0.016^{+0.010}_{-0.007}$	$0.014^{+0.006}_{-0.005}$	$0.012^{+0.006}_{-0.004}$
			0.138	0.036	0.024	0.015	0.021	0.017
0.8	0.2	0.0	$0.119^{+0.072}_{-0.049}$	$0.050^{+0.035}_{-0.021}$	$0.027^{+0.018}_{-0.011}$	$0.017^{+0.011}_{-0.006}$	$0.013^{+0.006}_{-0.004}$	$0.011^{+0.005}_{-0.003}$
			0.064	0.029	0.019	0.016	0.019	0.015
1.0	0.0	0.0	$0.044^{+0.021}_{-0.015}$	$0.033^{+0.022}_{-0.012}$	$0.019^{+0.013}_{-0.007}$	$0.013^{+0.008}_{-0.005}$	$0.009^{+0.005}_{-0.003}$	$0.009^{+0.004}_{-0.003}$

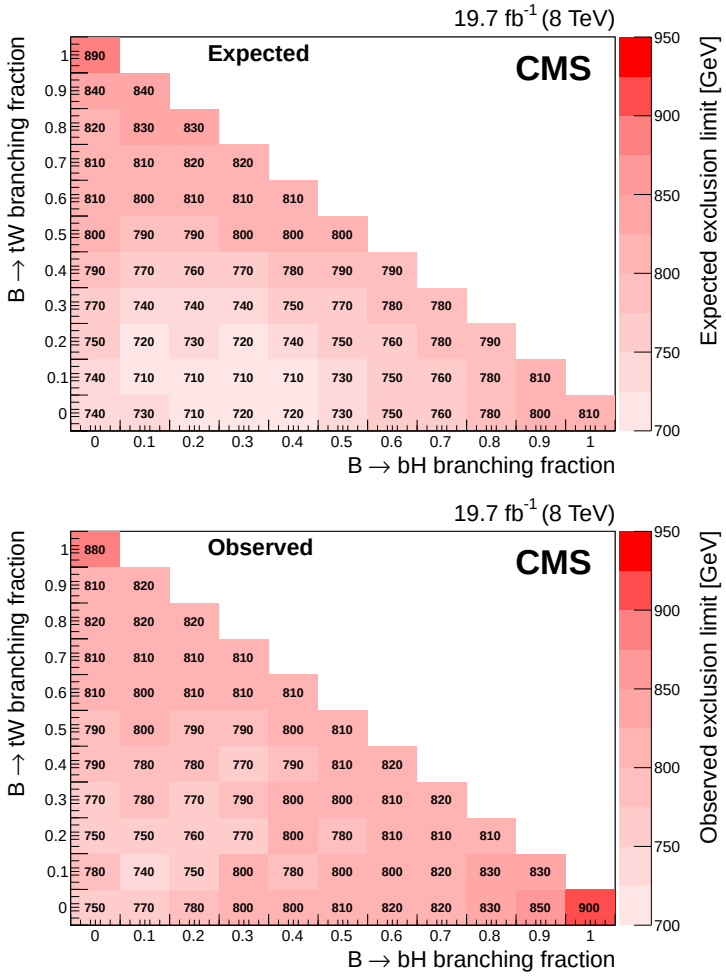

Figure 12: Expected (left) and observed (right) limits for each combination of branching fractions to tW, bZ, and bH obtained by the combination of channels. The color scale represents the mass exclusion limit obtained at each point. The branching fraction for the B quark decay to bZ can be obtained through the relation $\mathcal{B}(\mathrm{bZ}) = 1 - \mathcal{B}(\mathrm{tW}) - \mathcal{B}(\mathrm{bH})$.

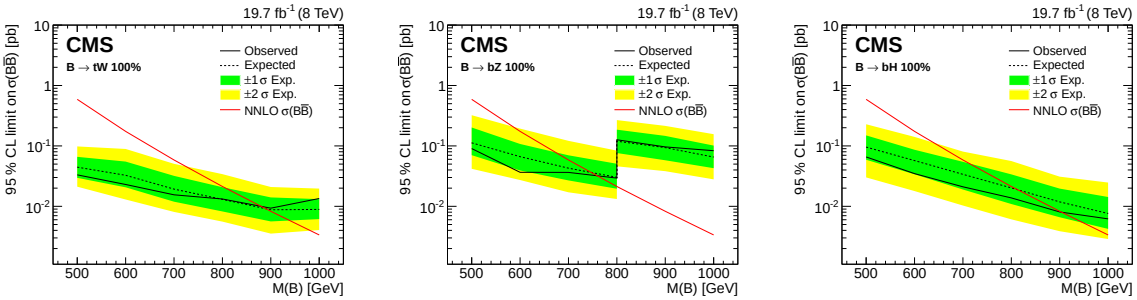

Figure 13: Observed and expected cross section limit results as a function of B mass, for the combination of all channels. The limit results are shown for exclusive branching fractions of B to tW (left), bZ (middle), and bH (right). The step observed in the bZ limit curve is due to two analysis channels (multilepton and OS dilepton) that do not contribute to the combination for B quark masses above 800 GeV.

Table 9: Expected and observed mass exclusion limits for the combined result, quoted at 95% CL, for the topologies where the B quark decays exclusively in one of the possible modes.

	95% CL $M(\mathrm{B})$ exclusion limit [GeV]	
	Expected	Observed
$\mathrm{B} \to \mathrm{tW}$	890	880
$\mathrm{B} \to \mathrm{bH}$	810	900
$\mathrm{B} \to \mathrm{bZ}$	740	750

Acknowledgments

We congratulate our colleagues in the CERN accelerator departments for the excellent performance of the LHC and thank the technical and administrative staffs at CERN and at other CMS institutes for their contributions to the success of the CMS effort. In addition, we gratefully acknowledge the computing centers and personnel of the Worldwide LHC Computing Grid for delivering so effectively the computing infrastructure essential to our analyses. Finally, we acknowledge the enduring support for the construction and operation of the LHC and the CMS detector provided by the following funding agencies: the Austrian Federal Ministry of Science, Research and Economy and the Austrian Science Fund; the Belgian Fonds de la Recherche Scientifique, and Fonds voor Wetenschappelijk Onderzoek; the Brazilian Funding Agencies (CNPq, CAPES, FAPERJ, and FAPESP); the Bulgarian Ministry of Education and Science; CERN; the Chinese Academy of Sciences, Ministry of Science and Technology, and National Natural Science Foundation of China; the Colombian Funding Agency (COLCIENCIAS); the Croatian Ministry of Science, Education and Sport, and the Croatian Science Foundation; the Research Promotion Foundation, Cyprus; the Ministry of Education and Research, Estonian Research Council via IUT23-4 and IUT23-6 and European Regional Development Fund, Estonia; the Academy of Finland, Finnish Ministry of Education and Culture, and Helsinki Institute of Physics; the Institut National de Physique Nucléaire et de Physique des Particules / CNRS, and Commissariat à l'Énergie Atomique et aux Énergies Alternatives / CEA, France; the Bundesministerium für Bildung und Forschung, Deutsche Forschungsgemeinschaft, and Helmholtz-Gemeinschaft Deutscher Forschungszentren, Germany; the General Secretariat for Research and Technology, Greece; the National Scientific Research Foundation, and National Innovation Office, Hungary; the Department of Atomic Energy and the Department of Science and Technology, India; the Institute for Studies in Theoretical Physics and Mathematics, Iran; the Science Foundation, Ireland; the Istituto Nazionale di Fisica Nucleare, Italy; the Ministry of Science, ICT and Future Planning, and National Research Foundation (NRF), Republic of Korea; the Lithuanian Academy of Sciences; the Ministry of Education, and University of Malaya (Malaysia); the Mexican Funding Agencies (CINVESTAV, CONACYT, SEP, and UASLP-FAI); the Ministry of Business, Innovation and Employment, New Zealand; the Pakistan Atomic Energy Commission; the Ministry of Science and Higher Education and the National Science Centre, Poland; the Fundação para a Ciência e a Tecnologia, Portugal; JINR, Dubna; the Ministry of Education and Science of the Russian Federation, the Federal Agency of Atomic Energy of the Russian Federation, Russian Academy of Sciences, and the Russian Foundation for Basic Research; the Ministry of Education, Science and Technological Development of Serbia; the Secretaría de Estado de Investigación, Desarrollo e Innovación and Programa Consolider-Ingenio 2010, Spain; the Swiss Funding Agencies (ETH Board, ETH Zurich, PSI, SNF, UniZH, Canton Zurich, and SER); the Ministry of Science and Technology, Taipei; the Thailand Center of Excellence in Physics, the Institute for the Promotion of Teaching Science and Technology of Thailand, Special Task Force for Activating Research and the National Science and Technology Development Agency of Thailand; the Scientific and Technical Research Council of Turkey, and Turkish Atomic Energy Authority; the National Academy of Sciences of Ukraine, and State Fund for Fundamental Researches, Ukraine; the Science and Technology Facilities Council, UK; the US Department of Energy, and the US National Science Foundation.

Individuals have received support from the Marie-Curie program and the European Research Council and EPLANET (European Union); the Leventis Foundation; the A. P. Sloan Foundation; the Alexander von Humboldt Foundation; the Belgian Federal Science Policy Office; the Fonds pour la Formation à la Recherche dans l'Industrie et dans l'Agriculture (FRIA-Belgium); the Agentschap voor Innovatie door Wetenschap en Technologie (IWT-Belgium); the Ministry

of Education, Youth and Sports (MEYS) of the Czech Republic; the Council of Science and Industrial Research, India; the HOMING PLUS program of the Foundation for Polish Science, cofinanced from European Union, Regional Development Fund; the Compagnia di San Paolo (Torino); the Consorzio per la Fisica (Trieste); MIUR project 20108T4XTM (Italy); the Thalis and Aristeia programs cofinanced by EU-ESF and the Greek NSRF; the National Priorities Research Program by Qatar National Research Fund; the Rachadapisek Sompot Fund for Postdoctoral Fellowship, Chulalongkorn University (Thailand); and the Welch Foundation.

References

[1] CMS Collaboration, "Observation of a new boson with mass near 125 GeV in pp collisions at $\sqrt{s}$ = 7 and 8 TeV", *JHEP* **06** (2013) 081, doi:10.1007/JHEP06(2013)081, arXiv:1303.4571.

[2] ATLAS Collaboration, "Observation of a new particle in the search for the Standard Model Higgs boson with the ATLAS detector at the LHC", *Phys. Lett. B* **716** (2012) 1, doi:10.1016/j.physletb.2012.08.020, arXiv:1207.7214.

[3] CMS Collaboration, "Observation of a new boson at a mass of 125 GeV with the CMS experiment at the LHC", *Phys. Lett. B* **716** (2012) 30, doi:10.1016/j.physletb.2012.08.021, arXiv:1207.7235.

[4] J. Bagger, S. Dimopoulos, and E. Masso, "Heavy families: Masses and mixings", *Nucl. Phys. B* **253** (1985) 397, doi:10.1016/0550-3213(85)90539-5.

[5] K. Agashe, R. Contino, and A. Pomarol, "The minimal composite Higgs model", *Nucl. Phys. B* **719** (2005) 165, doi:10.1016/j.nuclphysb.2005.04.035, arXiv:hep-ph/0412089.

[6] R. Contino, Y. Nomura, and A. Pomarol, "Higgs as a holographic pseudo-Goldstone boson", *Nucl. Phys. B* **671** (2003) 148, doi:10.1016/j.nuclphysb.2003.08.027, arXiv:hep-ph/0306259.

[7] J. Berger, J. Hubisz, and M. Perelstein, "A fermionic top partner: naturalness and the LHC", *JHEP* **07** (2012) 016, doi:10.1007/JHEP07(2012)016, arXiv:1205.0013.

[8] T. Han, H. E. Logan, and L.-T. Wang, "Smoking-gun signatures of little Higgs models", *JHEP* **01** (2006) 099, doi:10.1088/1126-6708/2006/01/099, arXiv:hep-ph/0506313.

[9] M. Perelstein, M. E. Peskin, and A. Pierce, "Top quarks and electroweak symmetry breaking in little Higgs models", *Phys. Rev. D* **69** (2004) 075002, doi:10.1103/PhysRevD.69.075002, arXiv:hep-ph/0310039.

[10] N. Arkani-Hamed et al., "The Minimal Moose for a Little Higgs", *JHEP* **08** (2002) 021, doi:10.1088/1126-6708/2002/08/021, arXiv:hep-ph/0206020.

[11] B. A. Dobrescu and C. T. Hill, "Electroweak symmetry breaking via top condensation seesaw", *Phys. Rev. Lett.* **81** (1998) 2634, doi:10.1103/PhysRevLett.81.2634, arXiv:hep-ph/9712319.

[12] J. A. Aguilar-Saavedra, R. Benbrik, S. Heinemeyer, and M. Pérez-Victoria, "Handbook of vectorlike quarks: Mixing and single production", *Phys. Rev. D* **88** (2013) 094010, doi:10.1103/PhysRevD.88.094010.

[13] S. Fajfer, A. Greljo, J. F. Kamenik, and I. Mustac, "Light Higgs and Vector-like Quarks without Prejudice", *JHEP* **07** (2013) 155, doi:10.1007/JHEP07(2013)155, arXiv:1304.4219.

[14] P. H. Frampton, P. Q. Hung, and M. Sher, "Quarks and leptons beyond the third generation", *Phys. Rept.* **330** (2000) 263, doi:10.1016/S0370-1573(99)00095-2, arXiv:hep-ph/9903387.

[15] A. Djouadi and A. Lenz, "Sealing the fate of a fourth generation of fermions", *Phys. Lett. B* **715** (2012) 310, doi:10.1016/j.physletb.2012.07.060.

[16] S. Gopalakrishna, T. Mandal, S. Mitra, and R. Tibrewala, "LHC signatures of a vector-like b'", *Phys. Rev. D* **84** (2011) 055001, doi:10.1103/PhysRevD.84.055001, arXiv:1107.4306.

[17] J. A. Aguilar-Saavedra, "Identifying top partners at LHC", *JHEP* **11** (2009) 030, doi:10.1088/1126-6708/2009/11/030, arXiv:0907.3155.

[18] Y. Okada and L. Panizzi, "LHC signatures of vector-like quarks", *Adv. High Energy Phys.* **2013** (2013) 364936, doi:10.1155/2013/364936, arXiv:1207.5607.

[19] P. Agrawal, S. D. Ellis, and W.-S. Hou, "Q→qZ decays at Tevatron and SSC energies", *Phys. Lett. B* **256** (1991) 289, doi:10.1016/0370-2693(91)90690-R.

[20] S. P. Martin, "Extra vector-like matter and the lightest Higgs scalar boson mass in low-energy supersymmetry", *Phys. Rev. D* **81** (2010) 035004, doi:10.1103/PhysRevD.81.035004, arXiv:0910.2732.

[21] CDF Collaboration, "Search for new particles leading to Z+jets final states in $p\bar{p}$ collisions at $\sqrt{s} = 1.96$ TeV", *Phys. Rev. D* **76** (2007) 072006, doi:10.1103/PhysRevD.76.072006, arXiv:0706.3264.

[22] ATLAS Collaboration, "Search for production of vector-like quark pairs and of four top quarks in the lepton-plus-jets final state in pp collisions at $\sqrt{s} = 8$ TeV with the ATLAS detector", *JHEP* **08** (2015) 105, doi:10.1007/JHEP08(2015)105, arXiv:1505.04306v2.

[23] CMS Collaboration, "The CMS experiment at the CERN LHC", *JINST* **3** (2008) S08004, doi:10.1088/1748-0221/3/08/S08004.

[24] F. Maltoni and T. Stelzer, "MadEvent: automatic event generation with MadGraph", *JHEP* **02** (2003) 027, doi:10.1088/1126-6708/2003/02/027, arXiv:hep-ph/0208156.

[25] J. Pumplin et al., "New generation of parton distributions with uncertainties from global QCD analysis", *JHEP* **07** (2002) 012, doi:10.1088/1126-6708/2002/07/012, arXiv:hep-ph/0201195.

[26] T. Sjöstrand, S. Mrenna, and P. Skands, "PYTHIA 6.4 physics and manual", *JHEP* **05** (2006) 026, doi:10.1088/1126-6708/2006/05/026, arXiv:hep-ph/0603175.

[27] P. Nason, "A new method for combining NLO QCD with shower Monte Carlo algorithms", *JHEP* **11** (2004) 040, doi:10.1088/1126-6708/2004/11/040, arXiv:hep-ph/0409146.

[28] S. Frixione, P. Nason, and C. Oleari, "Matching NLO QCD computations with Parton Shower simulations: the POWHEG method", *JHEP* **11** (2007) 070, doi:10.1088/1126-6708/2007/11/070, arXiv:0709.2092.

[29] S. Alioli, P. Nason, C. Oleari, and E. Re, "A general framework for implementing NLO calculations in shower Monte Carlo programs: the POWHEG BOX", *JHEP* **06** (2010) 043, doi:10.1007/JHEP06(2010)043, arXiv:1002.2581.

[30] S. Alioli, P. Nason, C. Oleari, and E. Re, "NLO single-top production matched with shower in POWHEG: s- and t-channel contributions", *JHEP* **09** (2009) 111, doi:10.1088/1126-6708/2009/09/111, arXiv:0907.4076. [Erratum: doi:10.1007/JHEP02(2010)011].

[31] R. Gavin, Y. Li, F. Petriello, and S. Quackenbush, "FEWZ 2.0: A code for hadronic Z production at next-to-next-to-leading order", *Comput. Phys. Commun.* **182** (2011) 2388, doi:10.1016/j.cpc.2011.06.008, arXiv:1011.3540.

[32] R. Gavin, Y. Li, F. Petriello, and S. Quackenbush, "W Physics at the LHC with FEWZ 2.1", *Comput. Phys. Commun.* **184** (2013) 208, doi:10.1016/j.cpc.2012.09.005, arXiv:1201.5896.

[33] Y. Li and F. Petriello, "Combining QCD and electroweak corrections to dilepton production in FEWZ", *Phys. Rev. D* **86** (2012) 094034, doi:10.1103/PhysRevD.86.094034, arXiv:1208.5967.

[34] M. Czakon, P. Fiedler, and A. Mitov, "Total Top-Quark Pair-Production Cross Section at Hadron Colliders Through $O(\alpha_S^4)$", *Phys. Rev. Lett.* **110** (2013) 252004, doi:10.1103/PhysRevLett.110.252004, arXiv:1303.6254.

[35] N. Kidonakis, "NNLL threshold resummation for top-pair and single-top production", *Phys. Part. Nucl.* **45** (2014) 714, doi:10.1134/S1063779614040091, arXiv:1210.7813.

[36] J. M. Campbell, R. K. Ellis, and K. Williams, "Vector boson pair production at the LHC", *JHEP* **07** (2011) 018, doi:10.1007/JHEP07(2011)018, arXiv:1105.0020.

[37] J. M. Campbell and R. K. Ellis, "$\mathrm{t\bar{t}}\,\mathrm{W}^{\pm}$ production and decay at NLO", *JHEP* **07** (2012), no. 052, doi:10.1007/JHEP07(2012)052.

[38] M. V. Garzelli, A. Kardos, C. G. Papadopoulos, and Z. Trócsányi, "$\mathrm{t\bar{t}W}^{\pm} + \mathrm{t\bar{t}Z}$ hadroproduction at NLO accuracy in QCD with Parton Shower and Hadronization effects", *JHEP* **11** (2012), no. 056, doi:10.1007/JHEP11(2012)056.

[39] M. Aliev et al., "HATHOR: HAdronic Top and Heavy quarks crOss section calculatoR", *Comput. Phys. Commun.* **182** (2011) 1034, doi:10.1016/j.cpc.2010.12.040, arXiv:1007.1327.

[40] M. Cacciari et al., "Top-pair production at hadron colliders with next-to-next-to-leading logarithmic soft-gluon resummation", *Phys. Lett. B* **710** (2012) 612, doi:10.1016/j.physletb.2012.03.013, arXiv:1111.5869.

[41] CMS Collaboration, "Particle–Flow Event Reconstruction in CMS and Performance for Jets, Taus, and $E_{\mathrm{T}}^{\mathrm{miss}}$", CMS Physics Analysis Summary CMS-PAS-PFT-09-001, 2009.

[42] CMS Collaboration, "Commissioning of the Particle-flow Event Reconstruction with the first LHC collisions recorded in the CMS detector", CMS Physics Analysis Summary CMS-PAS-PFT-10-001, 2010.

[43] CMS Collaboration, "Performance of electron reconstruction and selection with the CMS detector in proton-proton collisions at $\sqrt{s} = 8$ TeV", *JINST* **10** (2015) P06005, doi:10.1088/1748-0221/10/06/P06005, arXiv:1502.02701.

[44] CMS Collaboration, "Performance of CMS muon reconstruction in pp collision events at $\sqrt{s} = 7$ TeV", *JINST* **7** (2012) P10002, doi:10.1088/1748-0221/7/10/P10002, arXiv:1206.4071.

[45] CMS Collaboration, "Performance of τ-lepton reconstruction and identification in CMS", *J. Instrum.* **7** (2012) P01001, doi:10.1088/1748-0221/7/01/P01001.

[46] M. Cacciari and G. P. Salam, "Pileup subtraction using jet areas", *Phys. Lett. B* **659** (2008) 119, doi:10.1016/j.physletb.2007.09.077, arXiv:0707.1378.

[47] CMS Collaboration, "Commissioning of the Particle-Flow Reconstruction in Minimum-Bias and Jet Events from pp Collisions at 7 TeV", CMS Physics Analysis Summary CMS-PAS-PFT-10-002, 2010.

[48] M. Cacciari, G. P. Salam, and G. Soyez, "The anti-k_t jet clustering algorithm", *JHEP* **04** (2008) 063, doi:10.1088/1126-6708/2008/04/063, arXiv:0802.1189.

[49] CMS Collaboration, "Determination of Jet Energy Calibration and Transverse Momentum Resolution in CMS", *JINST* **6** (2011) P11002, doi:10.1088/1748-0221/6/11/P11002, arXiv:1107.4277.

[50] CMS Collaboration, "Identification of b-quark jets with the CMS experiment", *JINST* **8** (2013) 04013, doi:10.1088/1748-0221/8/04/P04013, arXiv:1211.4462.

[51] CMS Collaboration, "Performance of b tagging at $\sqrt{s} = 8$ TeV in multijet, $\mathrm{t\bar{t}}$ and boosted topology events", CMS Physics Analysis Summary CMS-PAS-BTV-13-001, 2013.

[52] Y. L. Dokshitzer, G. D. Leder, S. Moretti, and B. R. Webber, "Better jet clustering algorithms", *JHEP* **08** (1997) 001, doi:10.1088/1126-6708/1997/08/001, arXiv:hep-ph/9707323.

[53] M. Wobisch and T. Wengler, "Hadronization corrections to jet cross sections in deep-inelastic scattering", (1999). arXiv:hep-ph/9907280. DESY-PROC 1999-02.

[54] J. M. Butterworth, A. R. Davison, M. Rubin, and G. P. Salam, "Jet Substructure as a New Higgs-Search Channel at the Large Hadron Collider", *Phys. Rev. Lett.* **100** (2008) 242001, doi:10.1103/PhysRevLett.100.242001, arXiv:0802.2470.

[55] S. D. Ellis, C. K. Vermilion, and J. R. Walsh, "Recombination algorithms and jet substructure: Pruning as a tool for heavy particle searches", *Phys. Rev. D* **81** (2010) 094023, doi:10.1103/PhysRevD.81.094023, arXiv:0912.0033.

[56] J. Thaler and K. Van Tilburg, "Identifying boosted objects with N-subjettiness", *JHEP* **03** (2011) 015, doi:10.1007/JHEP03(2011)015, arXiv:1011.2268.

[57] CMS Collaboration, "Identification techniques for highly boosted W bosons that decay into hadrons", *JHEP* **12** (2014) 017, doi:10.1007/JHEP12(2014)017.

[58] CMS Collaboration, "CMS Luminosity Based on Pixel Cluster Counting – Summer 2013 Update", CMS Physics Analysis Summary CMS-PAS-LUM-13-001, 2013.

[59] CMS Collaboration, "Measurement of the differential cross section for top quark pair production in pp collisions at $\sqrt{s} = 8$ TeV", *Eur. Phys. J. C* **75** (2015), no. 11, 542, doi:10.1140/epjc/s10052-015-3709-x, arXiv:1505.04480.

[60] "HepData database, Durham". http://hepdata.net/record/ins1385104. doi:10.17182/hepdata.73428.

A The CMS Collaboration

Yerevan Physics Institute, Yerevan, Armenia
V. Khachatryan, A.M. Sirunyan, A. Tumasyan

Institut für Hochenergiephysik der OeAW, Wien, Austria
W. Adam, E. Asilar, T. Bergauer, J. Brandstetter, E. Brondolin, M. Dragicevic, J. Erö, M. Flechl, M. Friedl, R. Frühwirth[1], V.M. Ghete, C. Hartl, N. Hörmann, J. Hrubec, M. Jeitler[1], V. Knünz, A. König, M. Krammer[1], I. Krätschmer, D. Liko, T. Matsushita, I. Mikulec, D. Rabady[2], B. Rahbaran, H. Rohringer, J. Schieck[1], R. Schöfbeck, J. Strauss, W. Treberer-Treberspurg, W. Waltenberger, C.-E. Wulz[1]

National Centre for Particle and High Energy Physics, Minsk, Belarus
V. Mossolov, N. Shumeiko, J. Suarez Gonzalez

Universiteit Antwerpen, Antwerpen, Belgium
S. Alderweireldt, T. Cornelis, E.A. De Wolf, X. Janssen, A. Knutsson, J. Lauwers, S. Luyckx, S. Ochesanu, R. Rougny, M. Van De Klundert, H. Van Haevermaet, P. Van Mechelen, N. Van Remortel, A. Van Spilbeeck

Vrije Universiteit Brussel, Brussel, Belgium
S. Abu Zeid, F. Blekman, J. D'Hondt, N. Daci, I. De Bruyn, K. Deroover, N. Heracleous, J. Keaveney, S. Lowette, L. Moreels, A. Olbrechts, Q. Python, D. Strom, S. Tavernier, W. Van Doninck, P. Van Mulders, G.P. Van Onsem, I. Van Parijs

Université Libre de Bruxelles, Bruxelles, Belgium
P. Barria, C. Caillol, B. Clerbaux, G. De Lentdecker, H. Delannoy, D. Dobur, G. Fasanella, L. Favart, A.P.R. Gay, A. Grebenyuk, T. Lenzi, A. Léonard, T. Maerschalk, A. Mohammadi, L. Perniè, A. Randle-conde, T. Reis, T. Seva, C. Vander Velde, P. Vanlaer, J. Wang, R. Yonamine, F. Zenoni, F. Zhang[3]

Ghent University, Ghent, Belgium
K. Beernaert, L. Benucci, A. Cimmino, S. Crucy, A. Fagot, G. Garcia, M. Gul, J. Mccartin, A.A. Ocampo Rios, D. Poyraz, D. Ryckbosch, S. Salva, M. Sigamani, N. Strobbe, M. Tytgat, W. Van Driessche, E. Yazgan, N. Zaganidis

Université Catholique de Louvain, Louvain-la-Neuve, Belgium
S. Basegmez, C. Beluffi[4], O. Bondu, G. Bruno, R. Castello, A. Caudron, L. Ceard, G.G. Da Silveira, C. Delaere, D. Favart, L. Forthomme, A. Giammanco[5], J. Hollar, A. Jafari, P. Jez, M. Komm, V. Lemaitre, A. Mertens, C. Nuttens, L. Perrini, A. Pin, K. Piotrzkowski, A. Popov[6], L. Quertenmont, M. Selvaggi, M. Vidal Marono

Université de Mons, Mons, Belgium
N. Beliy, T. Caebergs, G.H. Hammad

Centro Brasileiro de Pesquisas Fisicas, Rio de Janeiro, Brazil
W.L. Aldá Júnior, G.A. Alves, L. Brito, M. Correa Martins Junior, T. Dos Reis Martins, C. Hensel, C. Mora Herrera, A. Moraes, M.E. Pol, P. Rebello Teles

Universidade do Estado do Rio de Janeiro, Rio de Janeiro, Brazil
E. Belchior Batista Das Chagas, W. Carvalho, J. Chinellato[7], A. Custódio, E.M. Da Costa, D. De Jesus Damiao, C. De Oliveira Martins, S. Fonseca De Souza, L.M. Huertas Guativa, H. Malbouisson, D. Matos Figueiredo, L. Mundim, H. Nogima, W.L. Prado Da Silva, A. Santoro, A. Sznajder, E.J. Tonelli Manganote[7], A. Vilela Pereira

Universidade Estadual Paulista [a], Universidade Federal do ABC [b], São Paulo, Brazil
S. Ahuja[a], C.A. Bernardes[b], A. De Souza Santos[b], S. Dogra[a], T.R. Fernandez Perez Tomei[a], E.M. Gregores[b], P.G. Mercadante[b], C.S. Moon[a,8], S.F. Novaes[a], Sandra S. Padula[a], D. Romero Abad, J.C. Ruiz Vargas

Institute for Nuclear Research and Nuclear Energy, Sofia, Bulgaria
A. Aleksandrov, V. Genchev[2], R. Hadjiiska, P. Iaydjiev, A. Marinov, S. Piperov, M. Rodozov, S. Stoykova, G. Sultanov, M. Vutova

University of Sofia, Sofia, Bulgaria
A. Dimitrov, I. Glushkov, L. Litov, B. Pavlov, P. Petkov

Institute of High Energy Physics, Beijing, China
M. Ahmad, J.G. Bian, G.M. Chen, H.S. Chen, M. Chen, T. Cheng, R. Du, C.H. Jiang, R. Plestina[9], F. Romeo, S.M. Shaheen, J. Tao, C. Wang, Z. Wang, H. Zhang

State Key Laboratory of Nuclear Physics and Technology, Peking University, Beijing, China
C. Asawatangtrakuldee, Y. Ban, Q. Li, S. Liu, Y. Mao, S.J. Qian, D. Wang, Z. Xu, W. Zou

Universidad de Los Andes, Bogota, Colombia
C. Avila, A. Cabrera, L.F. Chaparro Sierra, C. Florez, J.P. Gomez, B. Gomez Moreno, J.C. Sanabria

University of Split, Faculty of Electrical Engineering, Mechanical Engineering and Naval Architecture, Split, Croatia
N. Godinovic, D. Lelas, D. Polic, I. Puljak

University of Split, Faculty of Science, Split, Croatia
Z. Antunovic, M. Kovac

Institute Rudjer Boskovic, Zagreb, Croatia
V. Brigljevic, K. Kadija, J. Luetic, L. Sudic

University of Cyprus, Nicosia, Cyprus
A. Attikis, G. Mavromanolakis, J. Mousa, C. Nicolaou, F. Ptochos, P.A. Razis, H. Rykaczewski

Charles University, Prague, Czech Republic
M. Bodlak, M. Finger[10], M. Finger Jr.[10]

Academy of Scientific Research and Technology of the Arab Republic of Egypt, Egyptian Network of High Energy Physics, Cairo, Egypt
R. Aly[11], S. Aly[11], Y. Assran[12], S. Elgammal[13], A. Ellithi Kamel[14], A. Lotfy[15], M.A. Mahmoud[15], A. Radi[13,16], A. Sayed[16,13]

National Institute of Chemical Physics and Biophysics, Tallinn, Estonia
B. Calpas, M. Kadastik, M. Murumaa, M. Raidal, A. Tiko, C. Veelken

Department of Physics, University of Helsinki, Helsinki, Finland
P. Eerola, J. Pekkanen, M. Voutilainen

Helsinki Institute of Physics, Helsinki, Finland
J. Härkönen, V. Karimäki, R. Kinnunen, T. Lampén, K. Lassila-Perini, S. Lehti, T. Lindén, P. Luukka, T. Mäenpää, T. Peltola, E. Tuominen, J. Tuominiemi, E. Tuovinen, L. Wendland

Lappeenranta University of Technology, Lappeenranta, Finland
J. Talvitie, T. Tuuva

DSM/IRFU, CEA/Saclay, Gif-sur-Yvette, France
M. Besancon, F. Couderc, M. Dejardin, D. Denegri, B. Fabbro, J.L. Faure, C. Favaro, F. Ferri, S. Ganjour, A. Givernaud, P. Gras, G. Hamel de Monchenault, P. Jarry, E. Locci, M. Machet, J. Malcles, J. Rander, A. Rosowsky, M. Titov, A. Zghiche

Laboratoire Leprince-Ringuet, Ecole Polytechnique, IN2P3-CNRS, Palaiseau, France
S. Baffioni, F. Beaudette, P. Busson, L. Cadamuro, E. Chapon, C. Charlot, T. Dahms, O. Davignon, N. Filipovic, A. Florent, R. Granier de Cassagnac, S. Lisniak, L. Mastrolorenzo, P. Miné, I.N. Naranjo, M. Nguyen, C. Ochando, G. Ortona, P. Paganini, S. Regnard, R. Salerno, J.B. Sauvan, Y. Sirois, T. Strebler, Y. Yilmaz, A. Zabi

Institut Pluridisciplinaire Hubert Curien, Université de Strasbourg, Université de Haute Alsace Mulhouse, CNRS/IN2P3, Strasbourg, France
J.-L. Agram[17], J. Andrea, A. Aubin, D. Bloch, J.-M. Brom, M. Buttignol, E.C. Chabert, N. Chanon, C. Collard, E. Conte[17], X. Coubez, J.-C. Fontaine[17], D. Gelé, U. Goerlach, C. Goetzmann, A.-C. Le Bihan, J.A. Merlin[2], K. Skovpen, P. Van Hove

Centre de Calcul de l'Institut National de Physique Nucleaire et de Physique des Particules, CNRS/IN2P3, Villeurbanne, France
S. Gadrat

Université de Lyon, Université Claude Bernard Lyon 1, CNRS-IN2P3, Institut de Physique Nucléaire de Lyon, Villeurbanne, France
S. Beauceron, C. Bernet, G. Boudoul, E. Bouvier, S. Brochet, C.A. Carrillo Montoya, J. Chasserat, R. Chierici, D. Contardo, B. Courbon, P. Depasse, H. El Mamouni, J. Fan, J. Fay, S. Gascon, M. Gouzevitch, B. Ille, I.B. Laktineh, M. Lethuillier, L. Mirabito, A.L. Pequegnot, S. Perries, J.D. Ruiz Alvarez, D. Sabes, L. Sgandurra, V. Sordini, M. Vander Donckt, P. Verdier, S. Viret, H. Xiao

Georgian Technical University, Tbilisi, Georgia
T. Toriashvili[18]

Tbilisi State University, Tbilisi, Georgia
Z. Tsamalaidze[10]

RWTH Aachen University, I. Physikalisches Institut, Aachen, Germany
C. Autermann, S. Beranek, M. Edelhoff, L. Feld, A. Heister, M.K. Kiesel, K. Klein, M. Lipinski, A. Ostapchuk, M. Preuten, F. Raupach, J. Sammet, S. Schael, J.F. Schulte, T. Verlage, H. Weber, B. Wittmer, V. Zhukov[6]

RWTH Aachen University, III. Physikalisches Institut A, Aachen, Germany
M. Ata, M. Brodski, E. Dietz-Laursonn, D. Duchardt, M. Endres, M. Erdmann, S. Erdweg, T. Esch, R. Fischer, A. Güth, T. Hebbeker, C. Heidemann, K. Hoepfner, D. Klingebiel, S. Knutzen, P. Kreuzer, M. Merschmeyer, A. Meyer, P. Millet, M. Olschewski, K. Padeken, P. Papacz, T. Pook, M. Radziej, H. Reithler, M. Rieger, F. Scheuch, L. Sonnenschein, D. Teyssier, S. Thüer

RWTH Aachen University, III. Physikalisches Institut B, Aachen, Germany
V. Cherepanov, Y. Erdogan, G. Flügge, H. Geenen, M. Geisler, W. Haj Ahmad, F. Hoehle, B. Kargoll, T. Kress, Y. Kuessel, A. Künsken, J. Lingemann[2], A. Nehrkorn, A. Nowack, I.M. Nugent, C. Pistone, O. Pooth, A. Stahl

Deutsches Elektronen-Synchrotron, Hamburg, Germany
M. Aldaya Martin, I. Asin, N. Bartosik, O. Behnke, U. Behrens, A.J. Bell, K. Borras,

A. Burgmeier, A. Cakir, L. Calligaris, A. Campbell, S. Choudhury, F. Costanza, C. Diez Pardos, G. Dolinska, S. Dooling, T. Dorland, G. Eckerlin, D. Eckstein, T. Eichhorn, G. Flucke, E. Gallo, J. Garay Garcia, A. Geiser, A. Gizhko, P. Gunnellini, J. Hauk, M. Hempel[19], H. Jung, A. Kalogeropoulos, O. Karacheban[19], M. Kasemann, P. Katsas, J. Kieseler, C. Kleinwort, I. Korol, W. Lange, J. Leonard, K. Lipka, A. Lobanov, W. Lohmann[19], R. Mankel, I. Marfin[19], I.-A. Melzer-Pellmann, A.B. Meyer, G. Mittag, J. Mnich, A. Mussgiller, S. Naumann-Emme, A. Nayak, E. Ntomari, H. Perrey, D. Pitzl, R. Placakyte, A. Raspereza, P.M. Ribeiro Cipriano, B. Roland, M.Ö. Sahin, J. Salfeld-Nebgen, P. Saxena, T. Schoerner-Sadenius, M. Schröder, C. Seitz, S. Spannagel, K.D. Trippkewitz, C. Wissing

University of Hamburg, Hamburg, Germany
V. Blobel, M. Centis Vignali, A.R. Draeger, J. Erfle, E. Garutti, K. Goebel, D. Gonzalez, M. Görner, J. Haller, M. Hoffmann, R.S. Höing, A. Junkes, R. Klanner, R. Kogler, T. Lapsien, T. Lenz, I. Marchesini, D. Marconi, D. Nowatschin, J. Ott, F. Pantaleo[2], T. Peiffer, A. Perieanu, N. Pietsch, J. Poehlsen, D. Rathjens, C. Sander, H. Schettler, P. Schleper, E. Schlieckau, A. Schmidt, J. Schwandt, M. Seidel, V. Sola, H. Stadie, G. Steinbrück, H. Tholen, D. Troendle, E. Usai, L. Vanelderen, A. Vanhoefer

Institut für Experimentelle Kernphysik, Karlsruhe, Germany
M. Akbiyik, C. Amstutz, C. Barth, C. Baus, J. Berger, C. Beskidt, C. Böser, E. Butz, R. Caspart, T. Chwalek, F. Colombo, W. De Boer, A. Descroix, A. Dierlamm, R. Eber, M. Feindt, S. Fink, M. Fischer, F. Frensch, B. Freund, R. Friese, D. Funke, M. Giffels, A. Gilbert, D. Haitz, T. Harbaum, M.A. Harrendorf, F. Hartmann[2], U. Husemann, F. Kassel[2], I. Katkov[6], A. Kornmayer[2], S. Kudella, P. Lobelle Pardo, B. Maier, H. Mildner, M.U. Mozer, T. Müller, Th. Müller, M. Plagge, M. Printz, G. Quast, K. Rabbertz, S. Röcker, F. Roscher, I. Shvetsov, G. Sieber, H.J. Simonis, F.M. Stober, R. Ulrich, J. Wagner-Kuhr, S. Wayand, T. Weiler, S. Williamson, C. Wöhrmann, R. Wolf

Institute of Nuclear and Particle Physics (INPP), NCSR Demokritos, Aghia Paraskevi, Greece
G. Anagnostou, G. Daskalakis, T. Geralis, V.A. Giakoumopoulou, A. Kyriakis, D. Loukas, A. Markou, A. Psallidas, I. Topsis-Giotis

University of Athens, Athens, Greece
A. Agapitos, S. Kesisoglou, A. Panagiotou, N. Saoulidou, E. Tziaferi

University of Ioánnina, Ioánnina, Greece
I. Evangelou, G. Flouris, C. Foudas, P. Kokkas, N. Loukas, N. Manthos, I. Papadopoulos, E. Paradas, J. Strologas

Wigner Research Centre for Physics, Budapest, Hungary
G. Bencze, C. Hajdu, A. Hazi, P. Hidas, D. Horvath[20], F. Sikler, V. Veszpremi, G. Vesztergombi[21], A.J. Zsigmond

Institute of Nuclear Research ATOMKI, Debrecen, Hungary
N. Beni, S. Czellar, J. Karancsi[22], J. Molnar, Z. Szillasi

University of Debrecen, Debrecen, Hungary
M. Bartók[23], A. Makovec, P. Raics, Z.L. Trocsanyi, B. Ujvari

National Institute of Science Education and Research, Bhubaneswar, India
P. Mal, K. Mandal, N. Sahoo, S.K. Swain

Panjab University, Chandigarh, India
S. Bansal, S.B. Beri, V. Bhatnagar, R. Chawla, R. Gupta, U.Bhawandeep, A.K. Kalsi, A. Kaur, M. Kaur, R. Kumar, A. Mehta, M. Mittal, N. Nishu, J.B. Singh, G. Walia

University of Delhi, Delhi, India
Ashok Kumar, Arun Kumar, A. Bhardwaj, B.C. Choudhary, R.B. Garg, A. Kumar, S. Malhotra, M. Naimuddin, K. Ranjan, R. Sharma, V. Sharma

Saha Institute of Nuclear Physics, Kolkata, India
S. Banerjee, S. Bhattacharya, K. Chatterjee, S. Dey, S. Dutta, Sa. Jain, Sh. Jain, R. Khurana, N. Majumdar, A. Modak, K. Mondal, S. Mukherjee, S. Mukhopadhyay, A. Roy, D. Roy, S. Roy Chowdhury, S. Sarkar, M. Sharan

Bhabha Atomic Research Centre, Mumbai, India
A. Abdulsalam, R. Chudasama, D. Dutta, V. Jha, V. Kumar, A.K. Mohanty[2], L.M. Pant, P. Shukla, A. Topkar

Tata Institute of Fundamental Research, Mumbai, India
T. Aziz, S. Banerjee, S. Bhowmik[24], R.M. Chatterjee, R.K. Dewanjee, S. Dugad, S. Ganguly, S. Ghosh, M. Guchait, A. Gurtu[25], G. Kole, S. Kumar, B. Mahakud, M. Maity[24], G. Majumder, K. Mazumdar, S. Mitra, G.B. Mohanty, B. Parida, T. Sarkar[24], K. Sudhakar, N. Sur, B. Sutar, N. Wickramage[26]

Indian Institute of Science Education and Research (IISER), Pune, India
S. Sharma

Institute for Research in Fundamental Sciences (IPM), Tehran, Iran
H. Bakhshiansohi, H. Behnamian, S.M. Etesami[27], A. Fahim[28], R. Goldouzian, M. Khakzad, M. Mohammadi Najafabadi, M. Naseri, S. Paktinat Mehdiabadi, F. Rezaei Hosseinabadi, B. Safarzadeh[29], M. Zeinali

University College Dublin, Dublin, Ireland
M. Felcini, M. Grunewald

INFN Sezione di Bari [a], Università di Bari [b], Politecnico di Bari [c], Bari, Italy
M. Abbrescia[a,b], C. Calabria[a,b], C. Caputo[a,b], S.S. Chhibra[a,b], A. Colaleo[a], D. Creanza[a,c], L. Cristella[a,b], N. De Filippis[a,c], M. De Palma[a,b], L. Fiore[a], G. Iaselli[a,c], G. Maggi[a,c], M. Maggi[a], G. Miniello[a,b], S. My[a,c], S. Nuzzo[a,b], A. Pompili[a,b], G. Pugliese[a,c], R. Radogna[a,b], A. Ranieri[a], G. Selvaggi[a,b], L. Silvestris[a,2], R. Venditti[a,b], P. Verwilligen[a]

INFN Sezione di Bologna [a], Università di Bologna [b], Bologna, Italy
G. Abbiendi[a], C. Battilana[2], A.C. Benvenuti[a], D. Bonacorsi[a,b], S. Braibant-Giacomelli[a,b], L. Brigliadori[a,b], R. Campanini[a,b], P. Capiluppi[a,b], A. Castro[a,b], F.R. Cavallo[a], G. Codispoti[a,b], M. Cuffiani[a,b], G.M. Dallavalle[a], F. Fabbri[a], A. Fanfani[a,b], D. Fasanella[a,b], P. Giacomelli[a], C. Grandi[a], L. Guiducci[a,b], S. Marcellini[a], G. Masetti[a], A. Montanari[a], F.L. Navarria[a,b], A. Perrotta[a], A.M. Rossi[a,b], T. Rovelli[a,b], G.P. Siroli[a,b], N. Tosi[a,b], R. Travaglini[a,b]

INFN Sezione di Catania [a], Università di Catania [b], CSFNSM [c], Catania, Italy
G. Cappello[a], M. Chiorboli[a,b], S. Costa[a,b], F. Giordano[a], R. Potenza[a,b], A. Tricomi[a,b], C. Tuve[a,b]

INFN Sezione di Firenze [a], Università di Firenze [b], Firenze, Italy
G. Barbagli[a], V. Ciulli[a,b], C. Civinini[a], R. D'Alessandro[a,b], E. Focardi[a,b], S. Gonzi[a,b], V. Gori[a,b], P. Lenzi[a,b], M. Meschini[a], S. Paoletti[a], G. Sguazzoni[a], A. Tropiano[a,b], L. Viliani[a,b]

INFN Laboratori Nazionali di Frascati, Frascati, Italy
L. Benussi, S. Bianco, F. Fabbri, D. Piccolo

INFN Sezione di Genova [a], Università di Genova [b], Genova, Italy
V. Calvelli[a,b], F. Ferro[a], M. Lo Vetere[a,b], E. Robutti[a], S. Tosi[a,b]

INFN Sezione di Milano-Bicocca [a], Università di Milano-Bicocca [b], Milano, Italy
M.E. Dinardo[a,b], S. Fiorendi[a,b], S. Gennai[a], R. Gerosa[a,b], A. Ghezzi[a,b], P. Govoni[a,b], S. Malvezzi[a], R.A. Manzoni[a,b], B. Marzocchi[a,b,2], D. Menasce[a], L. Moroni[a], M. Paganoni[a,b], D. Pedrini[a], S. Ragazzi[a,b], N. Redaelli[a], T. Tabarelli de Fatis[a,b]

INFN Sezione di Napoli [a], Università di Napoli 'Federico II' [b], Napoli, Italy, Università della Basilicata [c], Potenza, Italy, Università G. Marconi [d], Roma, Italy
S. Buontempo[a], N. Cavallo[a,c], S. Di Guida[a,d,2], M. Esposito[a,b], F. Fabozzi[a,c], A.O.M. Iorio[a,b], G. Lanza[a], L. Lista[a], S. Meola[a,d,2], M. Merola[a], P. Paolucci[a,2], C. Sciacca[a,b], F. Thyssen

INFN Sezione di Padova [a], Università di Padova [b], Padova, Italy, Università di Trento [c], Trento, Italy
P. Azzi[a,2], N. Bacchetta[a], D. Bisello[a,b], A. Branca[a,b], R. Carlin[a,b], A. Carvalho Antunes De Oliveira[a,b], P. Checchia[a], M. Dall'Osso[a,b,2], T. Dorigo[a], U. Dosselli[a], F. Gasparini[a,b], U. Gasparini[a,b], A. Gozzelino[a], K. Kanishchev[a,c], S. Lacaprara[a], M. Margoni[a,b], A.T. Meneguzzo[a,b], J. Pazzini[a,b], N. Pozzobon[a,b], F. Simonetto[a,b], E. Torassa[a], M. Tosi[a,b], S. Ventura[a], M. Zanetti, P. Zotto[a,b], A. Zucchetta[a,b,2], G. Zumerle[a,b]

INFN Sezione di Pavia [a], Università di Pavia [b], Pavia, Italy
A. Braghieri[a], M. Gabusi[a,b], A. Magnani[a], S.P. Ratti[a,b], V. Re[a], C. Riccardi[a,b], P. Salvini[a], I. Vai[a], P. Vitulo[a,b]

INFN Sezione di Perugia [a], Università di Perugia [b], Perugia, Italy
L. Alunni Solestizi[a,b], M. Biasini[a,b], G.M. Bilei[a], D. Ciangottini[a,b,2], L. Fanò[a,b], P. Lariccia[a,b], G. Mantovani[a,b], M. Menichelli[a], A. Saha[a], A. Santocchia[a,b], A. Spiezia[a,b]

INFN Sezione di Pisa [a], Università di Pisa [b], Scuola Normale Superiore di Pisa [c], Pisa, Italy
K. Androsov[a,30], P. Azzurri[a], G. Bagliesi[a], J. Bernardini[a], T. Boccali[a], G. Broccolo[a,c], R. Castaldi[a], M.A. Ciocci[a,30], R. Dell'Orso[a], S. Donato[a,c,2], G. Fedi, L. Foà[a,c†], A. Giassi[a], M.T. Grippo[a,30], F. Ligabue[a,c], T. Lomtadze[a], L. Martini[a,b], A. Messineo[a,b], F. Palla[a], A. Rizzi[a,b], A. Savoy-Navarro[a,31], A.T. Serban[a], P. Spagnolo[a], P. Squillacioti[a,30], R. Tenchini[a], G. Tonelli[a,b], A. Venturi[a], P.G. Verdini[a]

INFN Sezione di Roma [a], Università di Roma [b], Roma, Italy
L. Barone[a,b], F. Cavallari[a], G. D'imperio[a,b,2], D. Del Re[a,b], M. Diemoz[a], S. Gelli[a,b], C. Jorda[a], E. Longo[a,b], F. Margaroli[a,b], P. Meridiani[a], F. Micheli[a,b], G. Organtini[a,b], R. Paramatti[a], F. Preiato[a,b], S. Rahatlou[a,b], C. Rovelli[a], F. Santanastasio[a,b], P. Traczyk[a,b,2]

INFN Sezione di Torino [a], Università di Torino [b], Torino, Italy, Università del Piemonte Orientale [c], Novara, Italy
N. Amapane[a,b], R. Arcidiacono[a,c], S. Argiro[a,b], M. Arneodo[a,c], R. Bellan[a,b], C. Biino[a], N. Cartiglia[a], M. Costa[a,b], R. Covarelli[a,b], P. De Remigis[a], A. Degano[a,b], N. Demaria[a], L. Finco[a,b,2], C. Mariotti[a], S. Maselli[a], G. Mazza[a], E. Migliore[a,b], V. Monaco[a,b], E. Monteil[a,b], M. Musich[a], M.M. Obertino[a,b], L. Pacher[a,b], N. Pastrone[a], M. Pelliccioni[a], G.L. Pinna Angioni[a,b], F. Ravera[a,b], A. Romero[a,b], M. Ruspa[a,c], R. Sacchi[a,b], A. Solano[a,b], A. Staiano[a]

INFN Sezione di Trieste [a], Università di Trieste [b], Trieste, Italy

S. Belforte[a], V. Candelise[a,b,2], M. Casarsa[a], F. Cossutti[a], G. Della Ricca[a,b], B. Gobbo[a], C. La Licata[a,b], M. Marone[a,b], A. Schizzi[a,b], T. Umer[a,b], A. Zanetti[a]

Kangwon National University, Chunchon, Korea
S. Chang, A. Kropivnitskaya, S.K. Nam

Kyungpook National University, Daegu, Korea
D.H. Kim, G.N. Kim, M.S. Kim, D.J. Kong, S. Lee, Y.D. Oh, A. Sakharov, D.C. Son

Chonbuk National University, Jeonju, Korea
J.A. Brochero Cifuentes, H. Kim, T.J. Kim, M.S. Ryu

Chonnam National University, Institute for Universe and Elementary Particles, Kwangju, Korea
S. Song

Korea University, Seoul, Korea
S. Choi, Y. Go, D. Gyun, B. Hong, M. Jo, H. Kim, Y. Kim, B. Lee, K. Lee, K.S. Lee, S. Lee, S.K. Park, Y. Roh

Seoul National University, Seoul, Korea
H.D. Yoo

University of Seoul, Seoul, Korea
M. Choi, J.H. Kim, J.S.H. Lee, I.C. Park, G. Ryu

Sungkyunkwan University, Suwon, Korea
Y. Choi, Y.K. Choi, J. Goh, D. Kim, E. Kwon, J. Lee, I. Yu

Vilnius University, Vilnius, Lithuania
A. Juodagalvis, J. Vaitkus

National Centre for Particle Physics, Universiti Malaya, Kuala Lumpur, Malaysia
I. Ahmed, Z.A. Ibrahim, J.R. Komaragiri, M.A.B. Md Ali[32], F. Mohamad Idris[33], W.A.T. Wan Abdullah

Centro de Investigacion y de Estudios Avanzados del IPN, Mexico City, Mexico
E. Casimiro Linares, H. Castilla-Valdez, E. De La Cruz-Burelo, I. Heredia-de La Cruz[34], A. Hernandez-Almada, R. Lopez-Fernandez, A. Sanchez-Hernandez

Universidad Iberoamericana, Mexico City, Mexico
S. Carrillo Moreno, F. Vazquez Valencia

Benemerita Universidad Autonoma de Puebla, Puebla, Mexico
S. Carpinteyro, I. Pedraza, H.A. Salazar Ibarguen

Universidad Autónoma de San Luis Potosí, San Luis Potosí, Mexico
A. Morelos Pineda

University of Auckland, Auckland, New Zealand
D. Krofcheck

University of Canterbury, Christchurch, New Zealand
P.H. Butler, S. Reucroft

National Centre for Physics, Quaid-I-Azam University, Islamabad, Pakistan
A. Ahmad, M. Ahmad, Q. Hassan, H.R. Hoorani, W.A. Khan, T. Khurshid, M. Shoaib

National Centre for Nuclear Research, Swierk, Poland
H. Bialkowska, M. Bluj, B. Boimska, T. Frueboes, M. Górski, M. Kazana, K. Nawrocki, K. Romanowska-Rybinska, M. Szleper, P. Zalewski

Institute of Experimental Physics, Faculty of Physics, University of Warsaw, Warsaw, Poland
G. Brona, K. Bunkowski, K. Doroba, A. Kalinowski, M. Konecki, J. Krolikowski, M. Misiura, M. Olszewski, M. Walczak

Laboratório de Instrumentação e Física Experimental de Partículas, Lisboa, Portugal
P. Bargassa, C. Beirão Da Cruz E Silva, A. Di Francesco, P. Faccioli, P.G. Ferreira Parracho, M. Gallinaro, L. Lloret Iglesias, F. Nguyen, J. Rodrigues Antunes, J. Seixas, O. Toldaiev, D. Vadruccio, J. Varela, P. Vischia

Joint Institute for Nuclear Research, Dubna, Russia
S. Afanasiev, P. Bunin, M. Gavrilenko, I. Golutvin, I. Gorbunov, A. Kamenev, V. Karjavin, V. Konoplyanikov, A. Lanev, A. Malakhov, V. Matveev[35], P. Moisenz, V. Palichik, V. Perelygin, S. Shmatov, S. Shulha, N. Skatchkov, V. Smirnov, A. Zarubin

Petersburg Nuclear Physics Institute, Gatchina (St. Petersburg), Russia
V. Golovtsov, Y. Ivanov, V. Kim[36], E. Kuznetsova, P. Levchenko, V. Murzin, V. Oreshkin, I. Smirnov, V. Sulimov, L. Uvarov, S. Vavilov, A. Vorobyev

Institute for Nuclear Research, Moscow, Russia
Yu. Andreev, A. Dermenev, S. Gninenko, N. Golubev, A. Karneyeu, M. Kirsanov, N. Krasnikov, A. Pashenkov, D. Tlisov, A. Toropin

Institute for Theoretical and Experimental Physics, Moscow, Russia
V. Epshteyn, V. Gavrilov, N. Lychkovskaya, V. Popov, I. Pozdnyakov, G. Safronov, A. Spiridonov, E. Vlasov, A. Zhokin

National Research Nuclear University 'Moscow Engineering Physics Institute' (MEPhI), Moscow, Russia
A. Bylinkin

P.N. Lebedev Physical Institute, Moscow, Russia
V. Andreev, M. Azarkin[37], I. Dremin[37], M. Kirakosyan, A. Leonidov[37], G. Mesyats, S.V. Rusakov, A. Vinogradov

Skobeltsyn Institute of Nuclear Physics, Lomonosov Moscow State University, Moscow, Russia
A. Baskakov, A. Belyaev, E. Boos, M. Dubinin[38], L. Dudko, A. Ershov, A. Gribushin, V. Klyukhin, O. Kodolova, I. Lokhtin, I. Myagkov, S. Obraztsov, S. Petrushanko, V. Savrin, A. Snigirev

State Research Center of Russian Federation, Institute for High Energy Physics, Protvino, Russia
I. Azhgirey, I. Bayshev, S. Bitioukov, V. Kachanov, A. Kalinin, D. Konstantinov, V. Krychkine, V. Petrov, R. Ryutin, A. Sobol, L. Tourtchanovitch, S. Troshin, N. Tyurin, A. Uzunian, A. Volkov

University of Belgrade, Faculty of Physics and Vinca Institute of Nuclear Sciences, Belgrade, Serbia
P. Adzic[39], M. Ekmedzic, J. Milosevic, V. Rekovic

Centro de Investigaciones Energéticas Medioambientales y Tecnológicas (CIEMAT), Madrid, Spain
J. Alcaraz Maestre, E. Calvo, M. Cerrada, M. Chamizo Llatas, N. Colino, B. De La Cruz, A. Delgado Peris, D. Domínguez Vázquez, A. Escalante Del Valle, C. Fernandez Bedoya, J.P. Fernández Ramos, J. Flix, M.C. Fouz, P. Garcia-Abia, O. Gonzalez Lopez, S. Goy Lopez, J.M. Hernandez, M.I. Josa, E. Navarro De Martino, A. Pérez-Calero Yzquierdo, J. Puerta Pelayo, A. Quintario Olmeda, I. Redondo, L. Romero, M.S. Soares

Universidad Autónoma de Madrid, Madrid, Spain
C. Albajar, J.F. de Trocóniz, M. Missiroli, D. Moran

Universidad de Oviedo, Oviedo, Spain
H. Brun, J. Cuevas, J. Fernandez Menendez, S. Folgueras, I. Gonzalez Caballero, E. Palencia Cortezon, J.M. Vizan Garcia

Instituto de Física de Cantabria (IFCA), CSIC-Universidad de Cantabria, Santander, Spain
I.J. Cabrillo, A. Calderon, J.R. Castiñeiras De Saa, J. Duarte Campderros, M. Fernandez, G. Gomez, A. Graziano, A. Lopez Virto, J. Marco, R. Marco, C. Martinez Rivero, F. Matorras, F.J. Munoz Sanchez, J. Piedra Gomez, T. Rodrigo, A.Y. Rodríguez-Marrero, A. Ruiz-Jimeno, L. Scodellaro, I. Vila, R. Vilar Cortabitarte

CERN, European Organization for Nuclear Research, Geneva, Switzerland
D. Abbaneo, E. Auffray, G. Auzinger, M. Bachtis, P. Baillon, A.H. Ball, D. Barney, A. Benaglia, J. Bendavid, L. Benhabib, J.F. Benitez, G.M. Berruti, G. Bianchi, P. Bloch, A. Bocci, A. Bonato, C. Botta, H. Breuker, T. Camporesi, G. Cerminara, S. Colafranceschi[40], M. D'Alfonso, D. d'Enterria, A. Dabrowski, V. Daponte, A. David, M. De Gruttola, F. De Guio, A. De Roeck, S. De Visscher, E. Di Marco, M. Dobson, M. Dordevic, T. du Pree, N. Dupont, A. Elliott-Peisert, J. Eugster, G. Franzoni, W. Funk, D. Gigi, K. Gill, D. Giordano, M. Girone, F. Glege, R. Guida, S. Gundacker, M. Guthoff, J. Hammer, M. Hansen, P. Harris, J. Hegeman, V. Innocente, P. Janot, H. Kirschenmann, M.J. Kortelainen, K. Kousouris, K. Krajczar, P. Lecoq, C. Lourenço, M.T. Lucchini, N. Magini, L. Malgeri, M. Mannelli, J. Marrouche, A. Martelli, L. Masetti, F. Meijers, S. Mersi, E. Meschi, F. Moortgat, S. Morovic, M. Mulders, M.V. Nemallapudi, H. Neugebauer, S. Orfanelli[41], L. Orsini, L. Pape, E. Perez, A. Petrilli, G. Petrucciani, A. Pfeiffer, D. Piparo, A. Racz, G. Rolandi[42], M. Rovere, M. Ruan, H. Sakulin, C. Schäfer, C. Schwick, A. Sharma, P. Silva, M. Simon, P. Sphicas[43], D. Spiga, J. Steggemann, B. Stieger, M. Stoye, Y. Takahashi, D. Treille, A. Tsirou, G.I. Veres[21], N. Wardle, H.K. Wöhri, A. Zagozdzinska[44], W.D. Zeuner

Paul Scherrer Institut, Villigen, Switzerland
W. Bertl, K. Deiters, W. Erdmann, R. Horisberger, Q. Ingram, H.C. Kaestli, D. Kotlinski, U. Langenegger, T. Rohe

Institute for Particle Physics, ETH Zurich, Zurich, Switzerland
F. Bachmair, L. Bäni, L. Bianchini, M.A. Buchmann, B. Casal, G. Dissertori, M. Dittmar, M. Donegà, M. Dünser, P. Eller, C. Grab, C. Heidegger, D. Hits, J. Hoss, G. Kasieczka, W. Lustermann, B. Mangano, A.C. Marini, M. Marionneau, P. Martinez Ruiz del Arbol, M. Masciovecchio, D. Meister, P. Musella, F. Nessi-Tedaldi, F. Pandolfi, J. Pata, F. Pauss, L. Perrozzi, M. Peruzzi, M. Quittnat, M. Rossini, A. Starodumov[45], M. Takahashi, V.R. Tavolaro, K. Theofilatos, R. Wallny, H.A. Weber

Universität Zürich, Zurich, Switzerland
T.K. Aarrestad, C. Amsler[46], M.F. Canelli, V. Chiochia, A. De Cosa, C. Galloni, A. Hinzmann,

T. Hreus, B. Kilminster, C. Lange, J. Ngadiuba, D. Pinna, P. Robmann, F.J. Ronga, D. Salerno, S. Taroni, Y. Yang

National Central University, Chung-Li, Taiwan
M. Cardaci, K.H. Chen, T.H. Doan, C. Ferro, M. Konyushikhin, C.M. Kuo, W. Lin, Y.J. Lu, R. Volpe, S.S. Yu

National Taiwan University (NTU), Taipei, Taiwan
R. Bartek, P. Chang, Y.H. Chang, Y.W. Chang, Y. Chao, K.F. Chen, P.H. Chen, C. Dietz, F. Fiori, U. Grundler, W.-S. Hou, Y. Hsiung, K.Y. Kao, Y.F. Liu, R.-S. Lu, M. Miñano Moya, E. Petrakou, J.F. Tsai, Y.M. Tzeng

Chulalongkorn University, Faculty of Science, Department of Physics, Bangkok, Thailand
B. Asavapibhop, K. Kovitanggoon, G. Singh, N. Srimanobhas, N. Suwonjandee

Cukurova University, Adana, Turkey
A. Adiguzel, S. Cerci[47], C. Dozen, S. Girgis, G. Gokbulut, Y. Guler, E. Gurpinar, I. Hos, E.E. Kangal[48], A. Kayis Topaksu, G. Onengut[49], K. Ozdemir[50], S. Ozturk[51], B. Tali[47], H. Topakli[51], M. Vergili, C. Zorbilmez

Middle East Technical University, Physics Department, Ankara, Turkey
I.V. Akin, B. Bilin, S. Bilmis, B. Isildak[52], G. Karapinar[53], U.E. Surat, M. Yalvac, M. Zeyrek

Bogazici University, Istanbul, Turkey
E.A. Albayrak[54], E. Gülmez, M. Kaya[55], O. Kaya[56], T. Yetkin[57]

Istanbul Technical University, Istanbul, Turkey
K. Cankocak, S. Sen[58], F.I. Vardarlı

Institute for Scintillation Materials of National Academy of Science of Ukraine, Kharkov, Ukraine
B. Grynyov

National Scientific Center, Kharkov Institute of Physics and Technology, Kharkov, Ukraine
L. Levchuk, P. Sorokin

University of Bristol, Bristol, United Kingdom
R. Aggleton, F. Ball, L. Beck, J.J. Brooke, E. Clement, D. Cussans, H. Flacher, J. Goldstein, M. Grimes, G.P. Heath, H.F. Heath, J. Jacob, L. Kreczko, C. Lucas, Z. Meng, D.M. Newbold[59], S. Paramesvaran, A. Poll, T. Sakuma, S. Seif El Nasr-storey, S. Senkin, D. Smith, V.J. Smith

Rutherford Appleton Laboratory, Didcot, United Kingdom
K.W. Bell, A. Belyaev[60], C. Brew, R.M. Brown, D.J.A. Cockerill, J.A. Coughlan, K. Harder, S. Harper, E. Olaiya, D. Petyt, C.H. Shepherd-Themistocleous, A. Thea, L. Thomas, I.R. Tomalin, T. Williams, W.J. Womersley, S.D. Worm

Imperial College, London, United Kingdom
M. Baber, R. Bainbridge, O. Buchmuller, A. Bundock, D. Burton, S. Casasso, M. Citron, D. Colling, L. Corpe, N. Cripps, P. Dauncey, G. Davies, A. De Wit, M. Della Negra, P. Dunne, A. Elwood, W. Ferguson, J. Fulcher, D. Futyan, G. Hall, G. Iles, G. Karapostoli, M. Kenzie, R. Lane, R. Lucas[59], L. Lyons, A.-M. Magnan, S. Malik, J. Nash, A. Nikitenko[45], J. Pela, M. Pesaresi, K. Petridis, D.M. Raymond, A. Richards, A. Rose, C. Seez, P. Sharp†, A. Tapper, K. Uchida, M. Vazquez Acosta[61], T. Virdee, S.C. Zenz

Brunel University, Uxbridge, United Kingdom
J.E. Cole, P.R. Hobson, A. Khan, P. Kyberd, D. Leggat, D. Leslie, I.D. Reid, P. Symonds, L. Teodorescu, M. Turner

Baylor University, Waco, USA
A. Borzou, J. Dittmann, K. Hatakeyama, A. Kasmi, H. Liu, N. Pastika

The University of Alabama, Tuscaloosa, USA
O. Charaf, S.I. Cooper, C. Henderson, P. Rumerio

Boston University, Boston, USA
A. Avetisyan, T. Bose, C. Fantasia, D. Gastler, P. Lawson, D. Rankin, C. Richardson, J. Rohlf, J. St. John, L. Sulak, D. Zou

Brown University, Providence, USA
J. Alimena, E. Berry, S. Bhattacharya, D. Cutts, N. Dhingra, A. Ferapontov, A. Garabedian, U. Heintz, E. Laird, G. Landsberg, Z. Mao, M. Narain, S. Sagir, T. Sinthuprasith

University of California, Davis, Davis, USA
R. Breedon, G. Breto, M. Calderon De La Barca Sanchez, S. Chauhan, M. Chertok, J. Conway, R. Conway, P.T. Cox, R. Erbacher, M. Gardner, W. Ko, R. Lander, M. Mulhearn, D. Pellett, J. Pilot, F. Ricci-Tam, S. Shalhout, J. Smith, M. Squires, D. Stolp, M. Tripathi, S. Wilbur, R. Yohay

University of California, Los Angeles, USA
R. Cousins, P. Everaerts, C. Farrell, J. Hauser, M. Ignatenko, G. Rakness, D. Saltzberg, E. Takasugi, V. Valuev, M. Weber

University of California, Riverside, Riverside, USA
K. Burt, R. Clare, J. Ellison, J.W. Gary, G. Hanson, J. Heilman, M. Ivova PANEVA, P. Jandir, E. Kennedy, F. Lacroix, O.R. Long, A. Luthra, M. Malberti, M. Olmedo Negrete, A. Shrinivas, S. Sumowidagdo, H. Wei, S. Wimpenny

University of California, San Diego, La Jolla, USA
J.G. Branson, G.B. Cerati, S. Cittolin, R.T. D'Agnolo, A. Holzner, R. Kelley, D. Klein, J. Letts, I. Macneill, D. Olivito, S. Padhi, M. Pieri, M. Sani, V. Sharma, S. Simon, M. Tadel, Y. Tu, A. Vartak, S. Wasserbaech[62], C. Welke, F. Würthwein, A. Yagil, G. Zevi Della Porta

University of California, Santa Barbara, Santa Barbara, USA
D. Barge, J. Bradmiller-Feld, C. Campagnari, A. Dishaw, V. Dutta, K. Flowers, M. Franco Sevilla, P. Geffert, C. George, F. Golf, L. Gouskos, J. Gran, J. Incandela, C. Justus, N. Mccoll, S.D. Mullin, J. Richman, D. Stuart, I. Suarez, W. To, C. West, J. Yoo

California Institute of Technology, Pasadena, USA
D. Anderson, A. Apresyan, A. Bornheim, J. Bunn, Y. Chen, J. Duarte, A. Mott, H.B. Newman, C. Pena, M. Pierini, M. Spiropulu, J.R. Vlimant, S. Xie, R.Y. Zhu

Carnegie Mellon University, Pittsburgh, USA
V. Azzolini, A. Calamba, B. Carlson, T. Ferguson, Y. Iiyama, M. Paulini, J. Russ, M. Sun, H. Vogel, I. Vorobiev

University of Colorado Boulder, Boulder, USA
J.P. Cumalat, W.T. Ford, A. Gaz, F. Jensen, A. Johnson, M. Krohn, T. Mulholland, U. Nauenberg, J.G. Smith, K. Stenson, S.R. Wagner

Cornell University, Ithaca, USA
J. Alexander, A. Chatterjee, J. Chaves, J. Chu, S. Dittmer, N. Eggert, N. Mirman, G. Nicolas

Kaufman, J.R. Patterson, A. Rinkevicius, A. Ryd, L. Skinnari, L. Soffi, W. Sun, S.M. Tan, W.D. Teo, J. Thom, J. Thompson, J. Tucker, Y. Weng, P. Wittich

Fermi National Accelerator Laboratory, Batavia, USA
S. Abdullin, M. Albrow, J. Anderson, G. Apollinari, L.A.T. Bauerdick, A. Beretvas, J. Berryhill, P.C. Bhat, G. Bolla, K. Burkett, J.N. Butler, H.W.K. Cheung, F. Chlebana, S. Cihangir, V.D. Elvira, I. Fisk, J. Freeman, E. Gottschalk, L. Gray, D. Green, S. Grünendahl, O. Gutsche, J. Hanlon, D. Hare, R.M. Harris, J. Hirschauer, B. Hooberman, Z. Hu, S. Jindariani, M. Johnson, U. Joshi, A.W. Jung, B. Klima, B. Kreis, S. Kwan†, S. Lammel, J. Linacre, D. Lincoln, R. Lipton, T. Liu, R. Lopes De Sá, J. Lykken, K. Maeshima, J.M. Marraffino, V.I. Martinez Outschoorn, S. Maruyama, D. Mason, P. McBride, P. Merkel, K. Mishra, S. Mrenna, S. Nahn, C. Newman-Holmes, V. O'Dell, O. Prokofyev, E. Sexton-Kennedy, A. Soha, W.J. Spalding, L. Spiegel, L. Taylor, S. Tkaczyk, N.V. Tran, L. Uplegger, E.W. Vaandering, C. Vernieri, M. Verzocchi, R. Vidal, A. Whitbeck, F. Yang, H. Yin

University of Florida, Gainesville, USA
D. Acosta, P. Avery, P. Bortignon, D. Bourilkov, A. Carnes, M. Carver, D. Curry, S. Das, G.P. Di Giovanni, R.D. Field, M. Fisher, I.K. Furic, J. Hugon, J. Konigsberg, A. Korytov, J.F. Low, P. Ma, K. Matchev, H. Mei, P. Milenovic[63], G. Mitselmakher, L. Muniz, D. Rank, L. Shchutska, M. Snowball, D. Sperka, S. Wang, J. Yelton

Florida International University, Miami, USA
S. Hewamanage, S. Linn, P. Markowitz, G. Martinez, J.L. Rodriguez

Florida State University, Tallahassee, USA
A. Ackert, J.R. Adams, T. Adams, A. Askew, J. Bochenek, B. Diamond, J. Haas, S. Hagopian, V. Hagopian, M. Jenkins, K.F. Johnson, A. Khatiwada, H. Prosper, V. Veeraraghavan, M. Weinberg

Florida Institute of Technology, Melbourne, USA
V. Bhopatkar, M. Hohlmann, H. Kalakhety, D. Mareskas-palcek, T. Roy, F. Yumiceva

University of Illinois at Chicago (UIC), Chicago, USA
M.R. Adams, L. Apanasevich, D. Berry, R.R. Betts, I. Bucinskaite, R. Cavanaugh, O. Evdokimov, L. Gauthier, C.E. Gerber, D.J. Hofman, P. Kurt, C. O'Brien, I.D. Sandoval Gonzalez, C. Silkworth, P. Turner, N. Varelas, Z. Wu, M. Zakaria

The University of Iowa, Iowa City, USA
B. Bilki[64], W. Clarida, K. Dilsiz, S. Durgut, R.P. Gandrajula, M. Haytmyradov, V. Khristenko, J.-P. Merlo, H. Mermerkaya[65], A. Mestvirishvili, A. Moeller, J. Nachtman, H. Ogul, Y. Onel, F. Ozok[54], A. Penzo, C. Snyder, P. Tan, E. Tiras, J. Wetzel, K. Yi

Johns Hopkins University, Baltimore, USA
I. Anderson, B.A. Barnett, B. Blumenfeld, D. Fehling, L. Feng, A.V. Gritsan, P. Maksimovic, C. Martin, K. Nash, M. Osherson, M. Swartz, M. Xiao, Y. Xin

The University of Kansas, Lawrence, USA
P. Baringer, A. Bean, G. Benelli, C. Bruner, J. Gray, R.P. Kenny III, D. Majumder[66], M. Malek, M. Murray, D. Noonan, S. Sanders, R. Stringer, Q. Wang, J.S. Wood

Kansas State University, Manhattan, USA
I. Chakaberia, A. Ivanov, K. Kaadze, S. Khalil, M. Makouski, Y. Maravin, L.K. Saini, N. Skhirtladze, I. Svintradze, S. Toda

Lawrence Livermore National Laboratory, Livermore, USA
D. Lange, F. Rebassoo, D. Wright

University of Maryland, College Park, USA
C. Anelli, A. Baden, O. Baron, A. Belloni, B. Calvert, S.C. Eno, C. Ferraioli, J.A. Gomez, N.J. Hadley, S. Jabeen, R.G. Kellogg, T. Kolberg, J. Kunkle, Y. Lu, A.C. Mignerey, K. Pedro, Y.H. Shin, A. Skuja, M.B. Tonjes, S.C. Tonwar

Massachusetts Institute of Technology, Cambridge, USA
A. Apyan, R. Barbieri, A. Baty, K. Bierwagen, S. Brandt, W. Busza, I.A. Cali, Z. Demiragli, L. Di Matteo, G. Gomez Ceballos, M. Goncharov, D. Gulhan, G.M. Innocenti, M. Klute, D. Kovalskyi, Y.S. Lai, Y.-J. Lee, A. Levin, P.D. Luckey, C. Mcginn, X. Niu, C. Paus, D. Ralph, C. Roland, G. Roland, G.S.F. Stephans, K. Sumorok, M. Varma, D. Velicanu, J. Veverka, J. Wang, T.W. Wang, B. Wyslouch, M. Yang, V. Zhukova

University of Minnesota, Minneapolis, USA
B. Dahmes, A. Finkel, A. Gude, P. Hansen, S. Kalafut, S.C. Kao, K. Klapoetke, Y. Kubota, Z. Lesko, J. Mans, S. Nourbakhsh, N. Ruckstuhl, R. Rusack, N. Tambe, J. Turkewitz

University of Mississippi, Oxford, USA
J.G. Acosta, S. Oliveros

University of Nebraska-Lincoln, Lincoln, USA
E. Avdeeva, K. Bloom, S. Bose, D.R. Claes, A. Dominguez, C. Fangmeier, R. Gonzalez Suarez, R. Kamalieddin, J. Keller, D. Knowlton, I. Kravchenko, J. Lazo-Flores, F. Meier, J. Monroy, F. Ratnikov, J.E. Siado, G.R. Snow

State University of New York at Buffalo, Buffalo, USA
M. Alyari, J. Dolen, J. George, A. Godshalk, I. Iashvili, J. Kaisen, A. Kharchilava, A. Kumar, S. Rappoccio

Northeastern University, Boston, USA
G. Alverson, E. Barberis, D. Baumgartel, M. Chasco, A. Hortiangtham, A. Massironi, D.M. Morse, D. Nash, T. Orimoto, R. Teixeira De Lima, D. Trocino, R.-J. Wang, D. Wood, J. Zhang

Northwestern University, Evanston, USA
K.A. Hahn, A. Kubik, N. Mucia, N. Odell, B. Pollack, A. Pozdnyakov, M. Schmitt, S. Stoynev, K. Sung, M. Trovato, M. Velasco, S. Won

University of Notre Dame, Notre Dame, USA
A. Brinkerhoff, N. Dev, M. Hildreth, C. Jessop, D.J. Karmgard, N. Kellams, K. Lannon, S. Lynch, N. Marinelli, F. Meng, C. Mueller, Y. Musienko[35], T. Pearson, M. Planer, R. Ruchti, G. Smith, N. Valls, M. Wayne, M. Wolf, A. Woodard

The Ohio State University, Columbus, USA
L. Antonelli, J. Brinson, B. Bylsma, L.S. Durkin, S. Flowers, A. Hart, C. Hill, R. Hughes, K. Kotov, T.Y. Ling, B. Liu, W. Luo, D. Puigh, M. Rodenburg, B.L. Winer, H.W. Wulsin

Princeton University, Princeton, USA
O. Driga, P. Elmer, J. Hardenbrook, P. Hebda, S.A. Koay, P. Lujan, D. Marlow, T. Medvedeva, M. Mooney, J. Olsen, C. Palmer, P. Piroué, X. Quan, H. Saka, D. Stickland, C. Tully, J.S. Werner, A. Zuranski

University of Puerto Rico, Mayaguez, USA
S. Malik

Purdue University, West Lafayette, USA
V.E. Barnes, D. Benedetti, D. Bortoletto, L. Gutay, M.K. Jha, M. Jones, K. Jung, M. Kress, N. Leonardo, D.H. Miller, N. Neumeister, F. Primavera, B.C. Radburn-Smith, X. Shi, I. Shipsey, D. Silvers, J. Sun, A. Svyatkovskiy, F. Wang, W. Xie, L. Xu, J. Zablocki

Purdue University Calumet, Hammond, USA
N. Parashar, J. Stupak

Rice University, Houston, USA
A. Adair, B. Akgun, Z. Chen, K.M. Ecklund, F.J.M. Geurts, M. Guilbaud, W. Li, B. Michlin, M. Northup, B.P. Padley, R. Redjimi, J. Roberts, J. Rorie, Z. Tu, J. Zabel

University of Rochester, Rochester, USA
B. Betchart, A. Bodek, P. de Barbaro, R. Demina, Y. Eshaq, T. Ferbel, M. Galanti, A. Garcia-Bellido, P. Goldenzweig, J. Han, A. Harel, O. Hindrichs, A. Khukhunaishvili, G. Petrillo, M. Verzetti

The Rockefeller University, New York, USA
L. Demortier

Rutgers, The State University of New Jersey, Piscataway, USA
S. Arora, A. Barker, J.P. Chou, C. Contreras-Campana, E. Contreras-Campana, D. Duggan, D. Ferencek, Y. Gershtein, R. Gray, E. Halkiadakis, D. Hidas, E. Hughes, S. Kaplan, R. Kunnawalkam Elayavalli, A. Lath, S. Panwalkar, M. Park, S. Salur, S. Schnetzer, D. Sheffield, S. Somalwar, R. Stone, S. Thomas, P. Thomassen, M. Walker

University of Tennessee, Knoxville, USA
M. Foerster, G. Riley, K. Rose, S. Spanier, A. York

Texas A&M University, College Station, USA
O. Bouhali[67], A. Castaneda Hernandez, M. Dalchenko, M. De Mattia, A. Delgado, S. Dildick, R. Eusebi, W. Flanagan, J. Gilmore, T. Kamon[68], V. Krutelyov, R. Montalvo, R. Mueller, I. Osipenkov, Y. Pakhotin, R. Patel, A. Perloff, J. Roe, A. Rose, A. Safonov, A. Tatarinov, K.A. Ulmer[2]

Texas Tech University, Lubbock, USA
N. Akchurin, C. Cowden, J. Damgov, C. Dragoiu, P.R. Dudero, J. Faulkner, S. Kunori, K. Lamichhane, S.W. Lee, T. Libeiro, S. Undleeb, I. Volobouev

Vanderbilt University, Nashville, USA
E. Appelt, A.G. Delannoy, S. Greene, A. Gurrola, R. Janjam, W. Johns, C. Maguire, Y. Mao, A. Melo, P. Sheldon, B. Snook, S. Tuo, J. Velkovska, Q. Xu

University of Virginia, Charlottesville, USA
M.W. Arenton, S. Boutle, B. Cox, B. Francis, J. Goodell, R. Hirosky, A. Ledovskoy, H. Li, C. Lin, C. Neu, E. Wolfe, J. Wood, F. Xia

Wayne State University, Detroit, USA
C. Clarke, R. Harr, P.E. Karchin, C. Kottachchi Kankanamge Don, P. Lamichhane, J. Sturdy

University of Wisconsin, Madison, USA
D.A. Belknap, D. Carlsmith, M. Cepeda, A. Christian, S. Dasu, L. Dodd, S. Duric, E. Friis, B. Gomber, R. Hall-Wilton, M. Herndon, A. Hervé, P. Klabbers, A. Lanaro, A. Levine, K. Long,

R. Loveless, A. Mohapatra, I. Ojalvo, T. Perry, G.A. Pierro, G. Polese, I. Ross, T. Ruggles, T. Sarangi, A. Savin, A. Sharma, N. Smith, W.H. Smith, D. Taylor, N. Woods

†: Deceased
1: Also at Vienna University of Technology, Vienna, Austria
2: Also at CERN, European Organization for Nuclear Research, Geneva, Switzerland
3: Also at State Key Laboratory of Nuclear Physics and Technology, Peking University, Beijing, China
4: Also at Institut Pluridisciplinaire Hubert Curien, Université de Strasbourg, Université de Haute Alsace Mulhouse, CNRS/IN2P3, Strasbourg, France
5: Also at National Institute of Chemical Physics and Biophysics, Tallinn, Estonia
6: Also at Skobeltsyn Institute of Nuclear Physics, Lomonosov Moscow State University, Moscow, Russia
7: Also at Universidade Estadual de Campinas, Campinas, Brazil
8: Also at Centre National de la Recherche Scientifique (CNRS) - IN2P3, Paris, France
9: Also at Laboratoire Leprince-Ringuet, Ecole Polytechnique, IN2P3-CNRS, Palaiseau, France
10: Also at Joint Institute for Nuclear Research, Dubna, Russia
11: Now at Helwan University, Cairo, Egypt
12: Also at Suez University, Suez, Egypt
13: Also at British University in Egypt, Cairo, Egypt
14: Also at Cairo University, Cairo, Egypt
15: Now at Fayoum University, El-Fayoum, Egypt
16: Now at Ain Shams University, Cairo, Egypt
17: Also at Université de Haute Alsace, Mulhouse, France
18: Also at Tbilisi State University, Tbilisi, Georgia
19: Also at Brandenburg University of Technology, Cottbus, Germany
20: Also at Institute of Nuclear Research ATOMKI, Debrecen, Hungary
21: Also at Eötvös Loránd University, Budapest, Hungary
22: Also at University of Debrecen, Debrecen, Hungary
23: Also at Wigner Research Centre for Physics, Budapest, Hungary
24: Also at University of Visva-Bharati, Santiniketan, India
25: Now at King Abdulaziz University, Jeddah, Saudi Arabia
26: Also at University of Ruhuna, Matara, Sri Lanka
27: Also at Isfahan University of Technology, Isfahan, Iran
28: Also at University of Tehran, Department of Engineering Science, Tehran, Iran
29: Also at Plasma Physics Research Center, Science and Research Branch, Islamic Azad University, Tehran, Iran
30: Also at Università degli Studi di Siena, Siena, Italy
31: Also at Purdue University, West Lafayette, USA
32: Also at International Islamic University of Malaysia, Kuala Lumpur, Malaysia
33: Also at Malaysian Nuclear Agency, MOSTI, Kajang, Malaysia
34: Also at Consejo Nacional de Ciencia y Tecnología, Mexico city, Mexico
35: Also at Institute for Nuclear Research, Moscow, Russia
36: Also at St. Petersburg State Polytechnical University, St. Petersburg, Russia
37: Also at National Research Nuclear University 'Moscow Engineering Physics Institute' (MEPhI), Moscow, Russia
38: Also at California Institute of Technology, Pasadena, USA
39: Also at Faculty of Physics, University of Belgrade, Belgrade, Serbia
40: Also at Facoltà Ingegneria, Università di Roma, Roma, Italy
41: Also at National Technical University of Athens, Athens, Greece

42: Also at Scuola Normale e Sezione dell'INFN, Pisa, Italy
43: Also at University of Athens, Athens, Greece
44: Also at Warsaw University of Technology, Institute of Electronic Systems, Warsaw, Poland
45: Also at Institute for Theoretical and Experimental Physics, Moscow, Russia
46: Also at Albert Einstein Center for Fundamental Physics, Bern, Switzerland
47: Also at Adiyaman University, Adiyaman, Turkey
48: Also at Mersin University, Mersin, Turkey
49: Also at Cag University, Mersin, Turkey
50: Also at Piri Reis University, Istanbul, Turkey
51: Also at Gaziosmanpasa University, Tokat, Turkey
52: Also at Ozyegin University, Istanbul, Turkey
53: Also at Izmir Institute of Technology, Izmir, Turkey
54: Also at Mimar Sinan University, Istanbul, Istanbul, Turkey
55: Also at Marmara University, Istanbul, Turkey
56: Also at Kafkas University, Kars, Turkey
57: Also at Yildiz Technical University, Istanbul, Turkey
58: Also at Hacettepe University, Ankara, Turkey
59: Also at Rutherford Appleton Laboratory, Didcot, United Kingdom
60: Also at School of Physics and Astronomy, University of Southampton, Southampton, United Kingdom
61: Also at Instituto de Astrofísica de Canarias, La Laguna, Spain
62: Also at Utah Valley University, Orem, USA
63: Also at University of Belgrade, Faculty of Physics and Vinca Institute of Nuclear Sciences, Belgrade, Serbia
64: Also at Argonne National Laboratory, Argonne, USA
65: Also at Erzincan University, Erzincan, Turkey
66: Also at National Taiwan University (NTU), Taipei, Taiwan
67: Also at Texas A&M University at Qatar, Doha, Qatar
68: Also at Kyungpook National University, Daegu, Korea